Mechanical loading reveals an intrinsic cardiomyocyte stiffness contribution to diastolic dysfunction in murine cardiometabolic disease

Johannes V. Janssens[1,6], Antonia J.A. Raaijmakers[1], Parisa Koutsifeli[3], Kate L. Weeks[1,4], James R. Bell[1,5], Jennifer E. Van EyK[6], Claire L. Curl[1], Kimberley M. Mellor[2,3,1]and Lea M.D. Delbridge[1]

[1] Department of Anatomy & Physiology, University of Melbourne, Australia

[2] Department of Physiology, University of Auckland, New Zealand

[3] Auckland Bioengineering Institute, University of Auckland, New Zealand

[4]Baker Department of Cardiometabolic Health (Baker), , University of Melbourne, Australia

[5]Department of Microbiology, Anatomy, Physiology & Pharmacology, La Trobe University, Australia

[6]Smidt Heart Institute, Cedars-Sinai Medical Center, Los Angeles, USA.

Running Title: *Cardiomyocyte stiffness in diastolic dysfunction*

Key words: *cardiomyocyte; diastolic dysfunction; cardiometabolic disease; stiffness; relaxation; Ca^{2+} myofilament interaction*

Corresponding author:

Prof Lea MD Delbridge

Cardiac Phenomics Laboratory

Department of Anatomy and Physiology,

University of Melbourne, Australia.

lmd@unimelb.edu.au

ABSTRACT

Increasingly, cardiometabolic syndromes including diabetes and obesity, are associated with occurrence of heart failure with diastolic dysfunction – including heart failure with preserved ejection fraction (HFpEF) and diabetic cardiomyopathy. Diagnosis of heart failure with diastolic dysfunction is independently associated with higher incidence of adverse clinical events. There is currently no specific treatment for diastolic dysfunction and therapies to manage symptoms have limited efficacy. Understanding of the cardiomyocyte origins of diastolic dysfunction is an important priority to identify new therapeutics. The goal of this investigation was to experimentally define *in vitro* stiffness properties (stress/strain) of cardiomyocytes derived from hearts of animals exhibiting diastolic dysfunction *in vivo* in response to dietary induction of cardiometabolic disease.

Mice fed a high-fat-sugar-diet (HFSD vs control) for at least 25 weeks exhibited glucose intolerance, obesity and diastolic dysfunction *in vivo* (echo E/e'). Intact isolated paced cardiomyocytes were each functionally investigated in three states: non-loaded, loaded ('afterload') and stretched ('pre-load') configurations. Mean stiffness of HFSD cardiomyocytes was 70% higher than control. The E/e' doppler ratio for the origin hearts was elevated by 35%. A significant relationship was identified between the *in vitro* stiffness of single cardiomyocytes (Youngs Modulus) and the *in vivo* dysfunction severity (Doppler E/e').

In relation to lengthening/relaxation performance, in the loaded HFSD cardiomyocytes (vs CTRL) the decrement in maximal sarcomere lengthening rate was more accentuated. With stretch, the Ca^{2+} transient decay time course was prolonged. In addition for HFSD the pacing-associated stiffness elevation was further increased and diastolic sarcomere length decreased, although diastolic Ca^{2+} level was reduced. Our findings suggest a previously undescribed alteration in Ca^{2+}- myofilament interaction contributes to stiffness in HFSD cardiomyocytes.

This study provides the first quantitative analysis of intact cardiomyocyte stiffness and performance deficits associated with acquired cardiometabolic disease. The findings demonstrate that a component of the cardiac diastolic dysfunction in cardiometabolic disease derives from intrinsic cardiomyocyte mechanical abnormality. These data offer impetus for further investigation to achieve therapeutic targeting of the specific myofilament structural modifications conferring cardiomyocyte stiffness in cardiometabolic disease.

INTRODUCTION

Increasingly, cardiometabolic syndromes, including diabetes and obesity, are associated with occurrence of heart failure with a diastolic dysfunction patho-phenotype (Sotomi *et al.*, 2021). Diastolic dysfunction is characteristic of heart failure with preserved ejection fraction (HFpEF) which has now overtaken heart failure with reduced ejection fraction (HFrEF) comprising the majority of new heart failure diagnoses (McHugh *et al.*, 2019; Jackson *et al.*, 2022). Diastolic dysfunction is also linked with progression of diabetic cardiomyopathy (Patil *et al.*, 2011; Redfield, 2016). With both HFpEF and diabetic heart disease, early development of diastolic dysfunction can be detected even when other phenotypic features/comorbidities are heterogeneous (ie hypertrophy, dilation, natriuretic factor elevation, hypertension) (Kittleson *et al.*, 2023). Common clinical features of cardiometabolic syndromes, including obesity and insulin resistance, are independent risk factors for diastolic dysfunction as a prelude to heart failure (Rozenbaum *et al.*, 2019; Kamon *et al.*, 2020). Cardiometabolic syndromes can involve the 'silent' presence and progression of diastolic dysfunction for an extended period. Symptoms can be subclinical and/or detectable only in challenge conditions (ie as reduced diastolic reserve in exercise) or when exacerbated by co-morbidity (Leung *et al.*, 2015; Lam *et al.*, 2019). Diagnosis of heart failure with diastolic dysfunction is independently associated with higher incidence of adverse clinical events (Sotomi *et al.*, 2021). Notably, there is currently no specific treatment for diastolic dysfunction and/or HFpEF, and therapies to manage symptoms have limited efficacy (Delbridge *et al.*, 2022).

In diastolic dysfunction, the relaxation and filling phases of the cardiac cycle are impaired and the condition is generally described qualitatively as an increase in left ventricular wall 'stiffness' (or by decrease in compliance, the inverse of stiffness) (Daniels *et al.*, 2022; Janssens *et al.*, 2024). Clinically and experimentally, reduced compliance can be measured invasively as an elevation in left ventricular filling pressure or an increase in the gradient of the diastolic pressure-volume relationship. Non-invasively, on doppler echocardiogram, an increase in the E/e' ratio [of early (E) mitral valve blood flow rate to early mitral annulus tissue motion (e')] is an index used to identify diastolic abnormality (Lo & Thomas, 2010). Myocardial stiffness is considered to reflect myocardial extracellular matrix abnormalities linked with increased tissue fibrosis. While a component of reduced compliance likely reflects fibrotic infiltration, diastolic dysfunction can be identified in settings where there is no evidence of increased interstitial fibrosis burden (Curl *et al.*, 2018). There is growing appreciation that alterations of myocardial compliance in diastolic dysfunction disease states represents underlying intrinsic cardiomyocyte stiffness pathology which contributes to impaired relaxation and filling (Zhou & Pu, 2016; Villalobos Lizardi *et al.*, 2022). Understanding of the cardiomyocyte origins of diastolic dysfunction is an important priority to identify new molecular targets and to support the development of new diagnostics and therapeutics to reduce morbidity and mortality in cardiometabolic disease states.

98 Cardiomyocyte origins of diastolic dysfunction potentially comprise structural and operational components.
99 Evidence of molecular changes in sarcomeric and cytoskeletal elements is extensive (Villalobos Lizardi *et al.*,
100 2022; Loescher *et al.*, 2023). Operationally, the cardiac cycle of contraction and relaxation is driven by the
101 cyclic flux of cardiomyocyte activator Ca^{2+} to initiate contraction (myocyte sarcomere shortening) and to
102 allow relaxation (myocyte sarcomere lengthening). Much current knowledge of cardiomyocyte failure
103 dysfunction derives from myocytes isolated from tissues of hearts exhibiting systolic dysfunction of various
104 aetiologies, now characterized as HFrEF (van Heerebeek *et al.*, 2006; Curl *et al.*, 2018). The HFrEF isolated
105 intact cardiomyocyte exhibits reduced shortening and decreased amplitude Ca^{2+} activation transients when
106 paced *in vitro* to contract isotonically (ie free shortening & non-loaded). In systolic dysfunction, a disease
107 mechanism of cardiomyocyte activator Ca^{2+} deficit is consistently observed in non-loaded cardiomyocyte
108 studies and has been a phenotypic finding for cardiomyocytes of a range of animal models. Marked
109 increases in interstitial and perivascular fibrosis are common features of HFrEF, conferring myocardial ECM
110 stiffness (Luo & Anderson, 2013). As various cardiac intervention surgeries are common for HFrEF patients,
111 biopsy tissues have been relatively available and clinical confirmation of cardiomyocyte experimental
112 findings has been extensive. HFpEF surgical interventions are much less frequent and availability of HFpEF
113 tissue samples limited.
114
115 In diastolic dysfunction, specifically in HFpEF animal models, evidence is accumulating that Ca^{2+} deficit and
116 impaired isotonic shortening are not phenotypic (Kilfoil *et al.*, 2020). Indeed non-loaded cardiomyocyte
117 hypercontractility and elevated Ca^{2+} levels have been reported (Curl *et al.*, 2018; Louch, 2020). Thus current
118 experimental enquiry focusses on cardiomyocyte performance under loaded conditions. While the term
119 'stiffness' is used as a general descriptor of impaired compliance in a cardiovascular setting, it is more
120 formally specified quantitatively in physical science disciplines (Mirsky, 1976). Stiffness is defined as the
121 force per cross-sectional area (stress) developed with application of a normalized stretch or deformation
122 (strain) to a material. The ratio of stress/strain defines stiffness of the material and is known as 'Young's
123 Modulus'. In the cardiac setting, a stretch or deformation state is commonly described as 'loading' – for
124 example 'preload' (diastolic stretch) and 'afterload' (resistance to shortening). Depending on the
125 experimental design, stiffness behaviour of myocardial tissues, cardiomyocytes and/or sub cellular
126 cytoskeleton and sarcomere structures all potentially contribute to *in vivo* functional stiffness. Little is
127 known about how stiffness measured at different structural levels may determine function *in vivo* and how
128 stiffness elements are quantitatively changed in pathophysiology – in particular in acquired cardiometabolic
129 disease conditions. Thus, the goal of this investigation was to experimentally characterize *in vitro* stiffness
130 properties (stress/strain) of cardiomyocytes derived from hearts of animals exhibiting diastolic dysfunction
131 *in vivo* in response to dietary induction of cardiometabolic disease.
132

Mice fed a high-fat-sugar-diet (HFSD vs control) for at least 25 weeks demonstrated glucose intolerance, obesity and diastolic dysfunction *in vivo* (echo E/e'). Intact isolated paced cardiomyocytes were each functionally investigated in three states: non-loaded, loaded ('afterload') and stretched ('pre-load') configurations. Our findings suggest a previously undescribed alteration in Ca^{2+}- myofilament interaction contributes to stiffness in HFSD cardiomyocytes, potentially by selectively reducing cross-bridge deactivation rates and increasing the number of cycling cross-bridges during diastole.

140 **METHODS & MATERIALS**

141 **Animal model of cardiometabolic disease**

142 As a pre-clinical cardiometabolic disease model, the high-fat/sugar diet (HFSD) fed rodent recapitulates a
143 common and growing human disease phenotype (obesity, insulin resistance, glucose intolerance) and has
144 been established as a diastolic dysfunction model (Heather *et al.*, 2022). Cardiometabolic disease was
145 induced in male C57Bl/6J mice by a high fat/high sugar (HFSD) dietary intervention commencing at 8-9
146 weeks of age. Animals were randomized to experimental treatment groups and were group housed (> 4
147 animals per cage) in a temperature-controlled environment 21-23°C with 12 hour light/dark cycles. After a
148 1 week transitional feeding period (alternating feed periods), animals were fed a HFSD (43% kcal from fat,
149 200g/kg sucrose, SF04-001, Specialty Feeds) or control reference diet (CTRL: 16% kcal from fat, 100g/kg
150 sucrose, AIN93G, Specialty Feeds) for at least 25 weeks. All animal experiments were approved by the
151 University of Melbourne (School of Biomedical Sciences) Animal Ethics Committee and complied with the
152 guidelines and regulations of the Code of Practice for the Care and Use of Animals for Scientific Purposes
153 (National Health and Medical Research Council Australia).

154

155 **Glucose tolerance testing**

156 At 23-25 weeks of feeding, glucose tolerance testing was performed in mice following 6 hours fasting as
157 previously described (Chandramouli *et al.*, 2018). Baseline blood glucose levels were measured using an
158 Accu-Chek glucometer with a blood sample obtained from a needle prick to the tail vein. Glucose (1.5 g/kg
159 body weight) was injected i.p. and blood glucose was measured at 5, 15, 30, 60 and 90 minutes after the
160 glucose injection.

161

162 **Transthoracic echocardiography**

163 At 25-26 weeks of feeding, cardiac structure, systolic and diastolic function were evaluated by transthoracic
164 2-dimensional B- and M-mode and blood flow and tissue doppler echocardiography (GE Vivid 9; 15mHz i13L
165 linear array transducer) as described previously (Chandramouli *et al.*, 2018; Curl *et al.*, 2018). Briefly, mice
166 were lightly anesthetised with Isoflurane (1.5%; Baxter healthcare, Australia). Parasternal short axis view
167 was used to measure systolic parameters (interventricular septum IVS, left ventricular posterior wall LVPW,
168 left ventricular internal dimension LVID, fractional shortening FS, ejection fraction EF, heart rate HR). Pulse
169 wave Doppler and tissue Doppler scans were acquired from the apical 4 chamber view to assess LV diastolic
170 function parameters: velocity of early (E) and late (A) mitral inflow and early (e’) and late (a’) diastolic
171 velocity of mitral annulus. From these compound indices of diastolic function E/e’, E/A and e’/a’ were
172 calculated. In addition, the slope of the E wave was used to calculate mitral valve deceleration time. Three
173 consecutive cardiac cycles were sampled for each measurement.

174

175 **Cardiomyocyte preparation, structural and functional assessment**

176 A series of protocols were implemented to phenotype cardiomyocyte and sarcomere morphology, and
177 assess functional status in different contraction configurations and challenge settings.
178
179 ***Cardiomyocyte isolation, morphology & microfluorimetry.*** HFSD and CTRL left ventricular cardiomyocytes
180 were enzymatically isolated using methods previously described (Howlett *et al.*, 2006; Mellor *et al.*, 2011).
181 Briefly, the heart was excised, cannulated via the aorta, and subjected to retrograde perfusion on a
182 Langendorff apparatus with an oxygenated Ca^{2+} free buffer at 37°C for 10 minutes. The buffer was
183 composed of (in mM): 130 NaCl, 5 KCl, 0.33 NaH_2PO_4; 1 $MgCl_2$, 25 HEPES; 20 Glucose; 3 Na Pyruvate; 1 Na
184 Lactate. The Ca^{2+} free buffer was then supplemented with 0.66mg/mL collagenase (Worthington; Type II),
185 0.033mg/mL trypsin and 0.05mM $CaCl_2$ and perfusion continued for a further 10 minutes. The heart was
186 removed from the Langendorff apparatus, and the left ventricle was segmented into small pieces in a high
187 potassium solution composed of (in mM): 30 KCl, 90 KOH, 30 KH_2PO_4, 3 $MgSO_4$, 50 glutamic acid, 20
188 taurine, 0.5 EGTA, 10 glucose, and 10 HEPES. Single left ventricular cardiomyocytes were isolated via gentle
189 trituration. Viable cardiomyocytes were resuspended in HEPES-Krebs buffer (in mM); 146.2 NaCl, 4.69 KCl,
190 0.35 $NaH_2PO_4H_2O$, 1.05 $MgSO_47H_2O$, 10 HEPES, 11 glucose containing 1.8mM Ca^{2+} and were stored on a
191 rocking platform at room temperature. From each heart cell dimensions were collected from at least 50 rod
192 shaped cardiomyocytes using an inverted light microscope (Nikon) and calibrated eye piece as previously
193 described (Curl *et al.*, 2018). Cardiomyocyte volume was calculated by inserting experimentally determined
194 myocyte length and width values into the formula: volume =length x width x depth x multiplier 0.54
195 (elliptical area of the rectangle defined by width & length, (Satoh *et al.*, 1996)). Cardiomyocyte width: depth
196 ratio was assumed to be 1.44 (Natali *et al.*, 2001). Cardiomyocyte cross-sectional area (CSA) could be
197 calculated from measured width scaled for 2-dimensional geometry. (CSA = W [W/1.44] x 0.54 μm^2). An
198 aliquot of isolated cardiomyocyte suspension was pipetted into a cell chamber mounted on the stage of an
199 inverted fluorescence microscope (Motic AE31) and superfused with HEPES-Krebs solution with 2mM Ca^{2+},
200 37°C at a flow rate of 2ml/min. Cardiomyocyte sarcomere length and Ca^{2+} transients were simultaneously
201 recorded during isotonic contractions. Myocyte force development was evaluated in the same cells with
202 transducer attachment, using four protocols described below.
203
204 ***Characterizing cardiomyocyte diastolic function: non-loaded shortening measurements (isotonic), loaded***
205 ***force measurements (auxotonic), stretch responses and pacing challenge.*** Cardiomyocyte performance
206 was evaluated in several paced conditions: designated non-loaded, loaded and stretched. The 'non-loaded'
207 state refers to the absence of externally applied load (noting that sarcomeric and cytoskeletal structures do
208 constitute an underlying internal load).
209
210 Firstly, cardiomyocyte non-loaded (<u>isotonic)</u> sarcomere contractions (IonOptix SarcLen, Fast Fourier
211 Transform, FFT) and Ca^{2+} transients (Fura2-AM, 5µM microfluorimetry F340:380nm ratio) were

212 simultaneously measured at 2Hz, using a microscope diaphragm to define a rectangular intra-myocyte
213 region of interest as depicted **Fig. S1**. During contraction cycles, cardiomyocyte sarcomere length was
214 monitored within an intracellular region of interest defined by an adjustable diaphragm mounted in the
215 microscope optical tube (**Fig S1A**)
216
217 Secondly, to obtain loaded (auxotonic) contraction data (ie 'afterload'), each cardiomyocyte was attached
218 to a pair of glass fibres coated with a bio-adhesive (MyoTak, IonOptix, USA). Attachment sites were
219 positioned to be outside the sarcomere tracking region, closer to myocyte 'ends'. One glass fibre was
220 connected to a force transducer (fibre stiffness 20N/m, IonOptix, USA), and the other to a piezo motor
221 (Nano-drive, Mad City Labs Inc. WI, USA) to adjust cardiomyocyte length. With successful attachments,
222 cardiomyocytes were lifted from the coverslip using motorised micromanipulators (MC1000E, Siskiyou
223 Corporation, USA) attached to both the force transducer and the piezo-motor. Baseline auxotonic
224 contractions at 2Hz were recorded. Sarcomere length changes were measured using FFT as described
225 above. In addition, with glass fibre attachment, tracking of mean sarcomere shortening within a myocyte
226 segment delineated by the glass fibre edge positions could be performed in parallel.
227
228 Thirdly, auxotonic responses during a standardized stretch protocol ('pre-load') were recorded to measure
229 the effect of increasing diastolic cardiomyocyte/sarcomere basal length during pacing. A quasi 'stress-
230 length' relation was constructed for each myocyte (where stress = force/cross-sectional area). The 'stress-
231 length' relation represents a cellular equivalent to the conventional muscle 'force-length' relationship. Prior
232 to the commencement of the myocyte stretch measurements a protocol to calibrate the stretch step was
233 implemented. Four consecutive 0.5V input signals were delivered to the piezo-motor to determine a
234 calibration constant to define the percentage cell stretch for a given voltage. For each myocyte a
235 *Calibration Constant* was calculated as: *myocyte segment length change per peizomotor mV / sarcomere*
236 *count in segment* [where *myocyte sarcomere count = myocyte segment length (µm) / average diastolic*
237 *sarcomere length (µm)*]. To track the glass fibre position a real-time contrast detection algorithm (IonOptix -
238 EdgeLength) was focused on the internal edge of each of the glass fibres (**Fig. S1**) (Peyronnet *et al.*, 2017).
239 This enabled reproducible and comparable stretch steps to be applied to different cardiomyocyte
240 preparations (**Fig. S1**). Prior to the 'stress-length' protocol, a cell-specific calibration constant was applied to
241 yield a standardised stretch for each cardiomyocyte evaluated. The stress-length protocol involved
242 progressive stretch steps totaling an approximate 30% cell stretch (**Fig. S1**).
243
244 Lastly, the pacing was increased to 4Hz, a rate adaptation period allowed (2mins) and the stress-length
245 protocol was repeated. Sarcomere length, force development and intracellular Ca^{2+} transients were
246 simultaneously measured. In summary, the following parameters were measured: diastolic stress
247 (mN/mm^2), diastolic stress-length relation [(mN/mm^2) / (%$^-$ length change), diastolic stress-sarcomere

248 length relations ($mN/mm^2 . \mu m^{-1}$), sarcomere shortening (% diastolic SL), maximum sarcomere shortening
249 and lengthening velocity (µm/s). In addition, Ca^{2+} parameters were measured: diastolic Ca^{2+}, systolic Ca^{2+},
250 amplitude of the Ca^{2+} transient and time constant of decay of the Ca^{2+} transient (tau).
251
252 **Statistical analyses**
253 Data are presented as mean ± SEM and statistical analysis was performed using GraphPad Prism V9.5.1.
254 Cardiomyocyte stress-length and stress-SL relations were modelled with simple linear regression. For
255 comparison between two groups an unpaired student t-test was used. For assessment between two
256 groups at multiple points a one-way ANOVA with Bonferroni multiple comparisons post-hoc test was used.
257 Two-way ANOVA with Šídák's multiple comparisons post-hoc test was used for the evaluation of data
258 groups with two independent variables. Pearson Correlation analyses were used to assess statistical
259 significance of fitted linear regression lines. A p-value of <0.05 was considered statistically significant.
260 Analyses were performed using a blinded protocol.
261

262 **RESULTS**

263 **Systemic indicators of cardiometabolic disease and *in vivo* diastolic function in HFSD mice**

264 High fat /sugar-fed mice exhibited obesity and glucose intolerance. Relative to CTRL, HFSD mice body
265 weight was significantly elevated within 5 weeks of dietary intervention increasing over the study duration
266 by 50% relative to CTRL (**Fig. 1A**, CTRL: 29.5±0.5 vs. HFSD: 45.7±1.2g). After 23-24 weeks diet treatment,
267 glucose tolerance testing of a subset of the HFSD cohort was performed. Glucose intolerance in response to
268 intraperitoneal glucose administration was evidenced by increased area under the curve, an indicator of
269 systemic insulin resistance (**Fig. 1B**).

270

271 After confirming these key cardiometabolic disease characteristics in the HFSD mice, echocardiographic
272 functional evaluation was undertaken. Focusing on diastolic function evaluation (**Fig. 1C-G**), there was
273 reduced velocity of the mitral tissue annulus displacement (CTRL: 28.5±1.3, HFSD: 25.2±0.9 mm/s) and
274 increased early mitral blood inflow (CTRL: 476.8±19.9, HFSD: 554.6±16.8 mm/s) in HFSD myocardium.
275 Deceleration time of mitral inflow was shortened (CTRL: 31.5±2.2, HFSD: 19.7±1.5 ms) and E/e' ratio
276 increased, all observations consistent with reduced tissue compliance and diastolic dysfunction (CTRL:
277 16.7±1.0, HFSD: 22.3±1.5). No differences in systolic performance parameters were observed (**Table S1**),
278 confirming the primary *in vivo* phenotype of diastolic dysfunction. The next step was to evaluate the
279 cardiomyocyte involvement in dysfunction.

280

281 **Non-loaded cardiomyocyte shortening and lengthening in CTRL and HFSD treatments**

282 Single isolated cardiomyocytes were prepared from hearts of a subset of mice which underwent
283 echocardiographic analyses. For intact, non-loaded cardiomyocytes sarcomere shortening and lengthening
284 cycles were similar for CTRL and HFSD groups (**Fig. 2A**). Diastolic sarcomere length (SL) (**Fig. 2B**, CTRL:
285 1.71±0.01, HFSD: 1.72±0.01 µm) and peak sarcomere shortening (**Fig. 2C**, CTRL: 3.79±0.33, HFSD: 3.94±0.40
286 % diastolic SL) were not different between groups. Examination of sarcomere contraction kinetics (**Fig. 2D**
287 exemplar trace) showed that the maximum rate of lengthening (**Fig. 2E**, CTRL: 1.08±0.14, HFSD: 1.29±0.18
288 µm/s) and shortening (**Fig. 2F**, CTRL: -2.32±0.21, HFSD: -2.57±0.28 µm/s) did not differ between CTRL and
289 HFSD groups. Collectively these findings indicate that in the non-loaded setting no differences in CTRL and
290 HFSD cardiomyocyte systolic and diastolic isotonic performance were detected, a finding consistent with
291 our previous studies in fructose-fed mice (Mellor *et al.*, 2012).

292

293 **Non-loaded cardiomyocyte Ca^{2+} transient decay and sarcomere lengthening in CTRL and HFSD treatments**

294 Next, Ca^{2+} parameters were compared with cardiomyocyte sarcomere lengthening performance during
295 relaxation and diastole. No significant difference was evident between dietary treatment groups in the
296 diastolic Ca^{2+} (**Fig. 3A**, CTRL: 0.749±0.016, HFSD: 0.761±0.017 $F_{340:380}$) or time constant (tau) of Ca^{2+} transient
297 decay (**Fig.3B**, CTRL: 0.160±0.011, HFSD: 0.137±0.009 sec). Thus, the significant diastolic dysfunction

298 measured *in vivo* for the HFSD group was not observed in an isotonic non-loaded *in vitro* setting. Treatment
299 differences in Ca^{2+} transient systolic parameters were also undetectable (**Fig. 3C-E**). To reconcile the
300 impaired echocardiographic heart performance with absence of dysfunction in isotonically contracting
301 single cardiomyocytes, the next strategy was to assess single cardiomyocyte response to loading. A
302 common feature of cardiometabolic disease is elevation in afterload – ie elevated systemic resistance
303 potentially impeding myocardial pump function. To simulate this *in vitro*, mechanically loaded
304 cardiomyocyte performance was examined.
305
306 **Loaded cardiomyocyte sarcomere shortening and lengthening**
307 Immediately after non-loaded (isotonic) cardiomyocyte recordings, glass fibres were attached to
308 cardiomyocytes at longitudinal positions to permit auxotonic, loaded contraction measurements. This
309 manoeuvre was successful for about 20% of cardiomyocytes, due to delicacy involved in manual glass fibre-
310 myocyte manipulations. For cells successfully attached, the mean difference in sarcomere length measured
311 pre- and post-conversion to auxotonic mode was <0.02% diastolic length, indicating isotonic and auxotonic
312 sarcomere initial lengths were well matched. For attached cardiomyocytes, a comparison of sarcomere
313 shortening behaviour in loaded state could be made (using FFT) to directly match with data obtained non-
314 loaded state.
315
316 With loading, for all myocytes (both treatment groups), the sarcomere peak shortening was reduced and
317 shortening and lengthening kinetics slowed when compared with non-loaded performance (**Fig. 4A**). Mean
318 data showed that in response to loading, sarcomere shortening was reduced by ~34% (**Fig. 4B**, non-loaded:
319 0.075±0.008, loaded: 0.050±0.006 µm). Maximum rate of shortening was decreased by 58% (non-loaded: -
320 2.85±0.28, loaded: -1.20±0.18 µm; not shown), and maximum rate of lengthening by 66% (**Fig. 4C**, non-
321 loaded: 1.46±0.21, loaded: 0.52±0.10 µm/s). The reductions in extent of shortening and maximum rate of
322 lengthening were positively correlated (**Fig. 4D**) suggesting the possibility of common underlying
323 mechanisms. The more marked reductions in shortening and lengthening rates (almost double reduction in
324 peak shortening) indicates that these kinetics reflect the influence of factors beyond those impacting
325 shortening alone.
326
327 To assess this, the maximum rates of lengthening and shortening were normalised by peak shortening
328 amplitude to derive measures of rate parameters independent of shortening extent and thus to yield a
329 measure of 'deformation rate' - ie rate of length change, relative to length change (units µm x sec-1)/µm =
330 1/sec). The effect of loading on deformation rate was accentuated in HFSD group (significant ANOVA diet x
331 load interaction effect, **Fig. 4E**). A selective HFSD effect was determined as the differential between
332 matched 'loaded' and 'non-loaded' lengthening cardiomyocytes. The decrement in maximum rate of
333 lengthening for CTRL and HFSD is shown in **Fig. 4F**, highlighting the more pronounced slowing of maximal

334 lengthening rate in HFSD (CTRL: 7.38±1.15, HFSD: 12.70±2.23 1/s) in response to loading. Treatment
335 differences in deformation were not evident during the shortening phase (data not shown)**.** These findings
336 indicated an accentuated influence of load, specific to lengthening in HFSD cardiomyocytes, and could
337 reflect impaired subcellular relaxation processes specific to the HFSD myocardium. Based on these data
338 identifying different CTRL and HFSD origin cardiomyocyte responses in loaded state, we next investigated
339 the effect of stretch applied during loaded myocyte pacing, as a single myocyte paradigm simulating
340 ventricular filling resistance ie 'preload'.
341
342 **Cardiomyocyte force development: measuring strain & stress during progressive cardiomyocyte stretch**
343 A hallmark of diastolic dysfunction is an elevated diastolic pressure-volume relationship which describes
344 the increased resistance of the myocardial wall to chamber filling (Aurigemma *et al.*, 2006). We sought to
345 design a single cardiomyocyte version of this relationship (Fowler *et al.*, 2015), by applying standardized
346 stretch steps to paced, loaded cardiomyocytes, defining the steps as a % of non-stretched state (ie 'strain').
347 Diastolic force was measured simultaneously during length stretch steps. The force measured at every
348 strain increment was normalized by cross sectional area (CSA) to produce a measure of 'stress' (ie
349 force/CSA, mN/mm^2). Thus a sarcomere 'stress/strain' relation (ie force-length) was constructed for each
350 myocyte.
351
352 The protocols employed to generate stress-strain are depicted in **Fig. S1** and described in detail in the
353 Methods. **Fig. S1** show the stretch standardisation approach used to enable reproducible application of
354 strain (converting voltage signals to linear displacement) as a % length change (via individual myocyte
355 calibration constant calculation) to allow comparisons between different cardiomyocytes. The size of each
356 step change in length on sarcomere length was measured (FFT) and confirmed by tracking the intra-
357 cardiomyocyte segment between the glass fibres (**Fig. S1**). In some cases a direct sarcomere FFT measure
358 was not microscopically resolvable due to myocyte contraction responses which partially positioned some
359 area of the myocyte outside the optimal focal plane. In these situations it was always possible to calculate
360 segment length change. For the example shown, stretch steps were determined to be 2.75µm, and
361 converted to % sarcomere length (ie strain) using sarcomere count within intracellular region of interest
362 area **(Fig. S1C)**. A comparison of the variability of cell stretches performed using a uniform (pre-set) stretch
363 constant and the individually derived stretch calibration constant demonstrates that reproducibility is
364 optimized with usage of the individual stretch calibration constant data (**Fig. S1D**). Force, sarcomere length
365 and % stretch were measured simultaneously **(Fig. S1)**.
366
367 **Quantifying diastolic stiffness in CTRL vs HFSD cardiomyocytes using strain normalization methods**
368 Superimposed exemplar stress recordings are shown in **Fig. 5A** for CTRL and HFSD cardiomyocytes,
369 captured during a series of progressive stretches during a 100 sec period. The broken lines are aligned with

370 the diastolic stress step increments for each of the 2 myocytes (using the data points collected prior to the
371 transition to a new step) throughout the series of progressive stretches. A robust increase in systolic force
372 with stretch is also evident, indicative of length-dependent activation, the cardiomyocyte basis for the
373 Frank-Starling mechanism.
374
375 The formal definition of stiffness is the ratio of force per cross-sectional area (stress) normalized to the
376 extent of stretch deformation (ie strain) (Mirsky, 1976). Thus, in this experimental setting stiffness could be
377 visualized as the gradient of the linear plot derived from the cardiomyocyte diastolic stress-length relation.
378 Our stretch protocol methodology provided two approaches for stiffness calculation (as per Methods).
379
380 A first approach used FFT measurement of sarcomere length to track cardiomyocyte stretch and was
381 plotted according to the standardized stretch steps (in units µm). An alternative approach used percent
382 length change calculated as the length of the cardiomyocyte segment between the glass attachment fibres
383 divided by the initial distance between the fibres prior to stretch (in units % initial length).
384
385 Applying the first approach, a linear regression was performed to fit the data from which a slope value
386 could be derived. **Fig. 5B** depicts the average diastolic and systolic stress-sarcomere length relations for
387 CTRL cardiomyocytes only. To determine cardiomyocyte diastolic stiffness using FFT-computed sarcomere
388 length values, the gradient of the mean slope of the diastolic stress sarcomere-length relation for each
389 treatment group was calculated, using mean sarcomere length change (µm) as the denominator. This
390 gradient was significantly higher in HFSD myocytes compared to CTRL (**Fig. 6A**). The individual slope
391 gradients were used to calculate the mean diastolic stress / strain gradient (**Fig. 6B,** CTRL: 2.40±0.72, HFSD:
392 5.50±1.51 (mN/mm^2) / µm), $p = 0.07$) where there was a trend for a 2.3 fold increase in stiffness of HFSD
393 cardiomyocytes. The statistical power of this analysis was limited due to the difficulty in achieving
394 resolvable diastolic sarcomere lengths by FFT for all myocytes.
395
396 Applying the second approach, it was possible to construct stress – segment length (%) relations for all
397 myocytes from which stress data could be obtained. In **Fig. 6C**, the stress – segment length data for HFSD
398 and CTRL are shown, with a robustly significant difference detected in mean gradient values. In **Fig. 6D** the
399 diastolic stress/strain values calculated for the myocytes from the two treatment groups using this segment
400 approach are directly compared. The HFSD cardiomyocyte stiffness index derived using this approach was
401 increased by 70% compared with CTRL (**Fig. 6D**, CTRL: 0.0075±0.0016, HFSD: 0.0128±0.0016 ((mN/mm^2)/%
402 length).
403
404 To examine the relationship between intrinsic *in vitro* cardiomyocyte stiffness and *in vivo* diastolic
405 dysfunction, diastolic stiffness (slope of the diastolic stress-length relation) averaged per animal was

406 plotted against the E/e' index of diastolic dysfunction. There was a significant correlation between
407 cardiomyocyte stiffness and E/e' in HFSD and no evidence of a relationship for the CTRL group (**Fig.6E** CTRL:
408 p=ns, HFSD: p=0.0096, r^2=0.9213). These data support the interpretation that intrinsic cardiomyocyte
409 stiffness represents a definable and inherent component of diastolic dysfunction occurring *in vivo* in
410 cardiometabolic disease.
411
412 **Load dependence of Ca^{2+} transient decay in CTRL and HFSD cardiomyocytes**
413 To further understand the cardiomyocyte functional elements comprising increased intrinsic stiffness in
414 cardiopathology, the relationship between Ca^{2+} transient features and myofilament deactivation in
415 response to progressive stretch was evaluated. In the intact cardiomyocyte model these electro-mechanical
416 coupling processes are functional for interrogation (in contrast to the disrupted cytosolic environment
417 which characterizes permeabilized myocyte preparations). The Ca^{2+} transient decay features were
418 compared for isotonic and auxotonic basal states and also in response to progressive stretch.
419
420 In CTRL cardiomyocytes there was no difference in the time constant of transient decay (tau, 1/e) between
421 loaded and stretched state (20% increase in length, **Fig. 7C.** loaded 1.12±0.14; stretched 1.09±0.10 fold
422 change vs non-loaded reference 1.00±0.12). In HFSD cardiomyocytes the time constant of Ca^{2+} transient
423 decay was increased in stretched cardiomyocytes relative to non-loaded (**Fig. 7C**. non-loaded, 1.00±0.12;
424 loaded: 1.22±0.15; stretched 1.42±0.19 fold change). A trend for an interaction effect (p=0.0549) between
425 diet and load was observed, suggesting potential for a differential Ca^{2+} transient response to load between
426 CTRL and HFSD cardiomyocytes. The effects can be visualised in **Fig. 7A-B** where the mono-exponential
427 decay of exemplar Ca^{2+} transients is depicted. The shallower decay of the Ca^{2+} transient in the stretched
428 state (**Fig 7B**, HFSD) was apparent whereas the loaded and non-loaded decay traces were virtually
429 overlayed for CTRL cardiomyocytes (**Fig. 7B**). These data suggest that stretch may enhance a mechanism by
430 which the myofilaments bind Ca^{2+} for a prolonged duration during relaxation thus reducing Ca^{2+} availability
431 for extrusion from the cytosol.
432
433 **Pacing-induced $[Ca^{2+}]_i$ increase to examine potential for a cross-bridge derived stiffness mechanism**
434 A further mechanistic study to probe the potential relationship between Ca^{2+} and stiffness involved
435 perturbation of cytosolic Ca^{2+} cycling time. Elevating stimulation frequency is a recognized physiologic
436 strategy to increase diastolic Ca^{2+} levels and to apply increased cardiomyocyte workload. In response to
437 frequency elevation (2Hz to 4Hz) cardiomyocyte diastolic Ca^{2+} levels increased in both CTRL and HFSD (**Fig.
438 8A & B**) groups consistent with previous studies (Varian & Janssen, 2007; Eisner *et al.*, 2020). In the HFSD
439 cardiomyocytes this effect was markedly diminished and about half the mean magnitude of the Ca^{2+} shift
440 observed for CTRL myocytes (**Fig. 8C**. CTRL 0.111±0.017; HFSD 0.054±0.017, $F_{340:380}$, 2-way ANOVA
441 significant interaction effect). Frequency elevation was associated with a reduction in diastolic sarcomere

442 length in both CTRL (3%) and HFSD (5%) loaded cardiomyocytes (**Fig. 8D**. CTRL 2Hz: 1.69±0.01, CTRL
443 4Hz:1.64±0.020, HFSD 2Hz: 1.69±0.014, HFSD 4Hz: 1.61±0.023 µm).The combination of normal diastolic
444 sarcomere length reduction, concomitant with blunted diastolic Ca^{2+} increase in HFSD cardiomyocytes, may
445 indicate elevated diastolic responsiveness to Ca^{2+} in the HFSD cardiomyocyte.
446
447 While frequency elevation did not change the stress/strain relation in CTRL cardiomyocytes, a significant
448 increase in the stress/strain gradient was observed in HFSD cardiomyocytes (**Fig. 8E&F**. CTRL 2Hz:
449 0.006±0.002, CTRL 4Hz:0.007±0.002; HFSD 2Hz: 0.012±0.002, HFSD 4Hz: 0.014±0.002 (mN/mm^2) / %
450 length). This may indicate a larger population of cross-bridges contributing to diastolic stiffness at
451 heightened workloads in HFSD cardiomyocytes although other potential non-cross-bridge sources cannot
452 be excluded.
453
454

455 **DISCUSSION**

456 Here we provide the first quantitative analysis of intact cardiomyocyte stiffness and performance deficits
457 associated with acquired cardiometabolic disease. We demonstrate that a major component of the cardiac
458 diastolic dysfunction in cardiometabolic disease derives from intrinsic cardiomyocyte mechanical
459 abnormality.

460

461 The concept of myocardial stiffness is a frequently invoked qualitative descriptor of the pathophysiologic
462 phenotype characterizing diastolic dysfunction. Clinically and experimentally the echocardiography
463 parameter E/e' is used as an index of myocardial stiffness in disease diagnosis. The parameter E/e' is a
464 compound measure of cellular and extracellular matrix stiffness contributors. Despite consistent *in vivo*
465 findings, an understanding of the cardiomyocyte-specific contribution to tissue stiffness has been difficult
466 to identify. Using a series of intact single cell recording manoeuvres, we have established that the stiffness
467 characteristics of individual isolated cardiomyocytes from normal and dysfunctional hearts can be defined,
468 normalized and compared. Further, a significant relationship was identified between the mean stiffness of
469 single cardiomyocytes and the extent of the origin heart diastolic dysfunction (ie E/e' vs Young's Modulus).

470

471 To recapitulate briefly, cardiometabolic disease induced by dietary intervention in mice was characterized
472 by marked body weight elevation (50%, 'obesity') and glucose intolerance. *In vivo* echocardiography
473 diagnosed significant diastolic dysfunction with a 35% elevation of the E/e' in HFSD animals (**Figs.1 & 2**) in
474 absence of systolic functional deficit (**Table. S1**). In paced non-loaded conditions (freely shortening
475 'isotonic' state), the sarcomere contraction cycles & Ca^{2+} transients (fura-2) were similar in CTRL and HFSD
476 cardiomyocytes (**Figs. 2 & 3**). When the same cardiomyocytes were loaded, the peak shortening magnitude
477 and maximal lengthening rate~~s~~ (**Fig. 4A-C**) were reduced for both diet conditions. In HFSD cardiomyocytes
478 the reduction in lengthening rate (but not shortening) was accentuated (**Fig 4E & F**), indicating a selective
479 negative impact of loading on relaxation of the HFSD-derived cardiomyocytes. In HFSD cardiomyocytes
480 there was a larger increase in diastolic force per cross-sectional area (stress: mN/um^2) in response to
481 standardized step increases in length (strain: % initial length[um]) (**Fig. 5A-B & 6A-C**). From these data a
482 'stress/strain' parameter was determined, defining diastolic stiffness for each myocyte ie 'Youngs Modulus'
483 ([$mN/\mu m^2$]/[% initial length[µm]). Mean stiffness was 70% higher in cardiomyocytes of HFSD animals (**Fig.**
484 **6D**). Thus the increase in cardiomyocyte stiffness index was approximately double the elevation of the *in*
485 *vivo* E/e' dysfunction index. Using matched *in vivo* and *in vitro* data, a significant correlation was found
486 between diastolic dysfunction (E/e') and mean cardiomyocyte stiffness value for HFSD-diet animals, while
487 there was no relationship between these parameters in the myocytes of CTRL-diet fed group (**Fig. 6E**). To
488 evaluate possible influence of mechanical state on the Ca^{2+} transient, the mean transient decline
489 parameters (tau) from non-loaded, loaded and stretched cardiomyocytes were compared. In HFSD
490 cardiomyocytes the time constant of Ca^{2+} transient decay was increased in stretched cardiomyocytes

491 relative to non-loaded, a feature not observed in CTRL cardiomyocytes (**Fig. 7**). Finally, in response to an *in*
492 *vitro* pacing HFSD cardiomyocytes exhibited accentuated diastolic stiffness even with a smaller increase in
493 diastolic Ca^{2+} level (**Fig. 8**). Collectively, these findings may reveal a previously undescribed alteration in
494 Ca^{2+}-myofilament interactions indicative of-a cross-bridge component to cardiomyocyte stiffness in
495 cardiometabolic disease.
496
497 **Dietary model of acquired metabolic syndrome and cardiac diastolic disease**
498 High-fat/sugar diet feeding (ie 'western diet') has previously been shown experimentally to induce diastolic
499 dysfunction in rodents with prolongation of isovolumic relaxation time (Pulinilkunnil *et al.*, 2014; Dia *et al.*,
500 2020; Sowers *et al.*, 2020; Wingard *et al.*, 2021, 2021). This dietary regime employed in this study has been
501 well characterized as a model of diastolic dysfunction, with gradual development of metabolic disturbance
502 (stable rate of weight gain and mild hyperglycemia), with maintained systolic function (ejection fraction and
503 fractional shortening). As has been reported previously, over the time span of the dietary intervention
504 differential fibrosis is not observed (Daniels *et al.*, 2022; Wells *et al.*, 2023; data not shown).The data
505 presented here are consistent with clinical observations linking cardiometabolic disease and diastolic
506 dysfunction.
507
508 The finding of increased stiffness here is consistent with some aspects of prior experiments involving
509 animal feeding of obesogenic diets, using other rodent preparation types– including permeabilized
510 cardiomyocytes, tissue strips/papillary muscles, and non-paced cardiomyocytes (Leopoldo *et al.*, 2010;
511 Gonçalves *et al.*, 2016; Sowers *et al.*, 2020). Interestingly stiffness in those studies was attributed to titin or
512 extracellular matrix properties. Our protocol with intact single cardiomyocytes allows a mechanistic
513 extension of these previous findings (see later discussion).
514
515 **Loading the intact cardiomyocyte - functional deficits revealed in HFSD**
516 Isotonically contracting cardiomyocytes of CTRL and HFSD mice exhibited identical shortening-lengthening
517 cycles, but a distinctly different decrement in lengthening rate when exposed to load (ie auxotonic with
518 progressive resistive 'afterload' increase). Our findings show unequivocally that cardiomyocyte mechanical
519 dysfunction cannot be detected by analysis of isotonic shortening. With loading, the peak shortening
520 magnitude and the maximal lengthening rates were reduced for both CTRL and HFSD. In HFSD the
521 lengthening rate reduction was accentuated even when shortening extent was accounted for. These
522 findings indicated specific influence of loading on lengthening in HFSD cardiomyocytes and could reflect
523 impaired subcellular relaxation processes specific to the HFSD myocardium.
524
525 Others have demonstrated a physiological effect of loading on shortening in cardiac cells/tissues in
526 different species (using slow pacing and sub physiologic temperature conditions), although the pronounced

527 effect on relaxation is not consistently reported (Lab *et al.*, 1984; White *et al.*, 1995; Shimkunas *et al.*,
528 2021). This is consistent with *in vivo* human clinical observations where there is a strong inverse association
529 between late-systolic loading and left ventricular wall displacement velocity during early diastole (Borlaug
530 *et al.*, 2007). Importantly, increased dependence of relaxation on afterload is reported to be an *in vivo*
531 feature of heart failure (Eichhorn *et al.*, 1992; Gillebert *et al.*, 2000). Regarding the Ca^{2+} transient, in the
532 current study a subtle prolongation effect is observed in both CTRL and HFSD cardiomyocytes when loaded
533 (but not stretched) which is consistent with recently reported findings in rat LV trabeculae (Dowrick *et al.*,
534 2022). The variability in the sarcomere shortening recorded for both non-loaded and loaded
535 cardiomyocytes is notable (**Fig.4**) but consistent with other studies assessing relaxation rates in rodent
536 cardiomyocytes (Delbridge & Roos, 1997; Clark & Campbell, 2019).
537
538 **Characterizing cardiomyocyte stretch & pacing challenge responses**
539 In order to quantify intact single cardiomyocyte stiffness our approach was to apply a calibrated stretch
540 protocol, based on pre-measurement of a calibration constant for each myocyte, tracking changes in force
541 generation and cytosolic Ca^{2+} responses for each stretch step. This calibrated step-by-step approach
542 enabled the stress and strain data to be gathered from actively paced cardiomyocytes over extended
543 periods (ie 80-100sec) and computed to generate a definitive, comparative stiffness parameter for each
544 cardiomyocyte.
545
546 In the intact myocyte model, the internal cytosolic regulatory milieu is preserved and the
547 cytoskeletal/sarcomeric/organelle structural framework is intact. Thus contributions to diastolic 'stiffness'
548 reflect components of the structural passive resistance to deformation and the basal crossbridge derived
549 activity. Recent studies of permeabilized cardiac muscle strip bundles have explored the separate
550 contributions of mictrotubule, titin, actin-associated, sarcolemmal and desmin-linked components to
551 passive force development (Loescher *et al.*, 2023). Prior studies of 'skinned' or quiescent myocardial
552 preparations have also identified sources of passive stiffness, with titin a major stiffness component in
553 cardiometabolic disease (Leopoldo *et al.*, 2010; Hamdani *et al.*, 2013; Gonçalves *et al.*, 2016; Hopf *et al.*,
554 2018; Sowers *et al.*, 2020; Abdellatif *et al.*, 2021).
555
556 Our findings indicate involvement of a cytosolic Ca^{2+} component of the stretch response. Ca^{2+} fluorescence
557 analyses from these stretch protocols showed novel stretch-dependent prolongation of Ca^{2+} transient
558 decay in the HFSD cardiomyocytes. The time constant of Ca^{2+} transient decay increased with loading and
559 further with stretching – a feature not evident in CTRL cardiomyocytes which provides additional
560 mechanistic insight (discussion below).
561

562 The final pacing frequency protocol was implemented to apply a 'stress test' to the loaded cardiomyocytes
563 with the expectation of elevated diastolic Ca^{2+}, potentially revealing a cross-bridge stiffness component in
564 HFSD cardiomyocytes. With a doubling of pacing frequency, a significant increase in the stress/strain
565 gradient was observed in HFSD cardiomyocytes (only), and a similar reduction in diastolic sarcomere length
566 in both CTRL and HFSD was observed. While cardiomyocyte diastolic Ca^{2+} level increased in both CTRL and
567 HFSD – the HFSD increase was less marked than CTRL. This was a surprising finding, not previously
568 reported in any other model setting. A suggestion of Ca^{2+} hyper-sensitivity arises (Davis *et al.*, 2007)
569 amongst other explanations to consider.
570
571 **Mechanistic insights into cross-bridge derived stiffness**
572 In cardiometabolic disease, a cardiomyocyte stiffness contribution from intra-myocyte structural/passive
573 sources is undoubtedly substantial. In the intact cell, all this structural architecture is preserved, and all the
574 structures are vulnerable to functionally damaging post translational modifications in the free radical
575 myocyte soup. Titin, as the largest coded protein in the genome with hundreds of modifiable residue sites
576 (regulatory and non-regulatory), receives much attention. Isoform variants, and a multitude of polymorphic
577 genotypes likely also contribute to the stiffness signature. With this model, clearly the extracellular matrix
578 is not a direct player, although an effect of disrupted membrane-spanning integrins cannot be precluded.
579
580 Here we report that a cardiometabolic disease phenotype induced by obesogenic diet includes a 35%
581 increase in diastolic dysfunction (by echo E/e') which relates to a mean 70% increase in loaded
582 cardiomyocyte stiffness modulus. Several lines of evidence emerging from this study suggest that Ca^{2+} -
583 related mechanism/s may contribute to cardiomyocyte stiffness increase. Specifically, in the loaded HFSD
584 cardiomyocyte (vs CTRL):
585 a) load confers accentuated lengthening rate deficit
586 b) with stretch, the Ca^{2+} transient decay time course is prolonged
587 c) with more rapid pacing diastolic stiffness increases and sarcomere length decreases, although diastolic
588 Ca^{2+} is less elevated.
589 Together these cardiomyocyte phenotypes would be consistent with selective impairment of relaxation
590 rate, selective myofilament hyper-activation, impeded diastolic filling and reduced diastolic reserve.
591
592 This combination of observations is consistent with the notion that length-dependent cross-bridge
593 attachment is prolonged in HFSD cardiomyocytes (or conversely detachment is delayed). An alteration in
594 the 3D geometry of the low affinity Ca^{2+} binding pocket would produce this effect, by stabilizing Ca^{2+} in the
595 pocket for longer every activation cycle. A manifestation of this altered binding function could be apparent
596 Ca^{2+} hypersensitivity. The Ca^{2+} dissociation rate has been theorized as an effector of the transient decay
597 time-course (Robinson *et al.*, 2018). A role for the troponin complex in regulation of Ca^{2+} affinity is well

598 established (Chemla *et al.*, 2000). Further evidence of structural modifications of specific regions of TnI and
599 TnC which form and regulate this pocket is required. Our mass spectrometry studies provide proof of
600 concept of relevant post-translational modification types (Janssens *et al.*, 2018).
601
602 **Limitations**
603 Given the diastolic dysfunction goals of this study, investigations have primarily focused on cardiomyocyte
604 relaxation and lengthening behaviors. Diastolic and systolic interactions are important and additional
605 protocols are in development for these studies. In this regard, we defer to the extensive body of
606 developmental research undertaken to develop software and instrumentation to perform single
607 cardiomyocyte 'Pressure-Volume (PV) loops' (Helmes *et al.*, 2016). In their approach, which mimics the PV
608 loops in the intact myocardium, stretch is applied after relaxation has occurred by using a force clamp to
609 maintain a predefined diastolic force level. This approach has been used to discover that titin truncation
610 shifts the working sarcomere length range preserving diastolic stiffness at the expense of systolic
611 performance (Methawasin *et al.*, 2022) and that highly compliant titin allows cardiomyocytes to function at
612 high diastolic Ca^{2+} levels (Najafi *et al.*, 2019). Conceivably, this approach could also be used to evaluate the
613 temporal relationship between slow or incomplete relaxation and cardiomyocyte cross-bridge derived
614 stiffness in a semi-situ manner. Operator expertise is imperative with this system which to date has been
615 very productive in the hands of the developers.
616
617 In our work we have adopted a pragmatic approach, simpler to implement – although still very challenging
618 with about 20% isotonic-to-loaded myocyte conversion success rate. When animals have many months of
619 feeding history and cell isolation from older and diseased hearts is difficult, an optimized loading and
620 stretching approach is key. The two approaches have not been benchmarked, although it can be predicted
621 that the viscous components of stiffness are likely underestimated when stretches are slow and relatively
622 small such as in this study (Caporizzo & Prosser, 2021). The capacity to directly and reproducibly determine
623 Youngs Modulus (stress/strain) with a slow stretch routine has useful comparative value.
624
625 With ongoing research, our priority is to undertake longitudinal studies, including both sexes, to investigate
626 the relative timing of the emergence of *in vivo* and *in vitro* stiffness phenotypes as differences in Ca^{2+}
627 handling have previously been observed between control male and female rodents (Farrell *et al.*, 2010).
628 This has high translational relevance as we have previously identified a differential time course of diastolic
629 dysfunction development in females and males, with increased female vulnerability (Reichelt *et al.*, 2013;
630 Chandramouli *et al.*, 2018).
631
632 **In conclusion**

This is the first study to link elevated intact single cardiomyocyte stiffness with *in vivo* diastolic dysfunction in a diet-induced cardiometabolic disease mouse model. The novel findings identify augmented load dependence and reduced diastolic reserve as fundamental features of cardiomyocytes derived from hearts exhibiting cardiometabolic diastolic dysfunction. Taken together, the findings emphasise the importance of mechanical loading and pacing frequency in revealing latent diastolic abnormalities at the cardiomyocyte level. The rationale for further studies identifying specific subcellular and molecular mechanisms of cardiomyocyte stiffness in cardiometabolic disease prior to failure onset is compelling.

642 **REFERENCES**

643 Abdellatif M et al. (2021). Nicotinamide for the treatment of heart failure with preserved ejection fraction.
644 *Sci Transl Med* **13,** eabd7064.

645 Aurigemma GP, Zile MR & Gaasch WH (2006). Contractile Behavior of the Left Ventricle in Diastolic Heart
646 Failure. *Circulation* **113,** 296–304.

647 Borlaug BA, Melenovsky V, Redfield MM, Kessler K, Chang H-J, Abraham TP & Kass DA (2007). Impact of
648 Arterial Load and Loading Sequence on Left Ventricular Tissue Velocities in Humans. *Journal of the*
649 *American College of Cardiology* **50,** 1570–1577.

650 Caporizzo MA & Prosser BL (2021). Need for Speed: The Importance of Physiological Strain Rates in
651 Determining Myocardial Stiffness. *Front Physiol* **12,** 696694.

652 Chandramouli C, Reichelt ME, Curl CL, Varma U, Bienvenu LA, Koutsifeli P, Raaijmakers AJA, De Blasio MJ,
653 Qin CX, Jenkins AJ, Ritchie RH, Mellor KM & Delbridge LMD (2018). Diastolic dysfunction is more
654 apparent in STZ-induced diabetic female mice, despite less pronounced hyperglycemia. *Sci Rep* **8,**
655 2346.

656 Chemla D, Coirault C, Hébert J-L & Lecarpentier Y (2000). Mechanics of Relaxation of the Human Heart.
657 *Physiology* **15,** 78–83.

658 Clark JA & Campbell SG (2019). Diverse relaxation rates exist among rat cardiomyocytes isolated from a
659 single myocardial region. *J Physiol* **597,** 711–722.

660 Curl CL, Danes VR, Bell JR, Raaijmakers AJA, Ip WTK, Chandramouli C, Harding TW, Porrello ER, Erickson JR,
661 Charchar FJ, Kompa AR, Edgley AJ, Crossman DJ, Soeller C, Mellor KM, Kalman JM, Harrap SB &
662 Delbridge LMD (2018). Cardiomyocyte Functional Etiology in Heart Failure With Preserved Ejection
663 Fraction Is Distinctive-A New Preclinical Model. *J Am Heart Assoc* **7,** e007451.

664 Daniels LJ, Macindoe C, Koutsifeli P, Annandale M, Raaijmakers AJA, Weeks KL, Bell JR, Janssens JV, Curl CL,
665 Delbridge LMD & Mellor KM (2022). Myocardial deformation imaging by 2D speckle tracking
666 echocardiography for assessment of diastolic dysfunction in murine cardiopathology.
667 2022.08.06.503061. Available at: https://www.biorxiv.org/content/10.1101/2022.08.06.503061v1
668 [Accessed May 21, 2023].

669 Davis J, Wen H, Edwards T & Metzger JM (2007). Thin Filament Disinhibition by Restrictive Cardiomyopathy
670 Mutant R193H Troponin I Induces Ca2+-Independent Mechanical Tone and Acute Myocyte
671 Remodeling. *Circulation Research* **100,** 1494–1502.

672 Delbridge LM & Roos KP (1997). Optical methods to evaluate the contractile function of unloaded isolated
673 cardiac myocytes. *J Mol Cell Cardiol* **29,** 11–25.

674 Delbridge LMD, Bell JR, Weeks KL, Raaijmakers AJA & Mellor KM (2022). HFpEF etiology - Can focus on sex-
675 specific mechanisms deliver insights for all? *J Mol Cell Cardiol* **173,** 71–72.

676 Dia M, Gomez L, Thibault H, Tessier N, Leon C, Chouabe C, Ducreux S, Gallo-Bona N, Tubbs E, Bendridi N,
677 Chanon S, Leray A, Belmudes L, Couté Y, Kurdi M, Ovize M, Rieusset J & Paillard M (2020). Reduced
678 reticulum–mitochondria Ca2+ transfer is an early and reversible trigger of mitochondrial
679 dysfunctions in diabetic cardiomyopathy. *Basic Res Cardiol* **115,** 74.

680 Dowrick JM, Tran K, Garrett AS, Anderson AJ, Nielsen PMF, Taberner AJ & Han J-C (2022). Work-loop
681 contractions reveal that the afterload-dependent time course of cardiac Ca2+ transients is
682 modulated by preload. *Journal of Applied Physiology* **133,** 663–675.

683 Eichhorn EJ, Willard JE, Alvarez L, Kim AS, Glamann DB, Risser RC & Grayburn PA (1992). Are contraction
684 and relaxation coupled in patients with and without congestive heart failure? *Circulation* **85,** 2132–
685 2139.

686 Eisner DA, Caldwell JL, Trafford AW & Hutchings DC (2020). The Control of Diastolic Calcium in the Heart.
687 *Circ Res* **126,** 395–412.

688 Farrell SR, Ross JL & Howlett SE (2010). Sex differences in mechanisms of cardiac excitation-contraction
689 coupling in rat ventricular myocytes. *Am J Physiol Heart Circ Physiol* **299,** H36-45.

690 Fowler ED, Benoist D, Drinkhill MJ, Stones R, Helmes M, Wüst RCI, Stienen GJM, Steele DS & White E (2015).
691 Decreased creatine kinase is linked to diastolic dysfunction in rats with right heart failure induced
692 by pulmonary artery hypertension. *J Mol Cell Cardiol* **86,** 1–8.

693 Gillebert TC, Leite-Moreira AF & De Hert SG (2000). Load dependent diastolic dysfunction in heart failure.
694 *Heart Fail Rev* **5,** 345–355.

695 Gonçalves N, Silva AF, Rodrigues PG, Correia E, Moura C, Eloy C, Roncon-Albuquerque R, Falcão-Pires I &
696 Leite-Moreira AF (2016). Early cardiac changes induced by a hypercaloric Western-type diet in
697 "subclinical" obesity. *American Journal of Physiology-Heart and Circulatory Physiology* **310,** H655–
698 H666.

699 Hamdani N, Franssen C, Lourenço A, Falcão-Pires I, Fontoura D, Leite S, Plettig L, López B, Ottenheijm CA,
700 Becher PM, González A, Tschöpe C, Díez J, Linke WA, Leite-Moreira AF & Paulus WJ (2013).
701 Myocardial Titin Hypophosphorylation Importantly Contributes to Heart Failure With Preserved
702 Ejection Fraction in a Rat Metabolic Risk Model. *Circulation: Heart Failure* **6,** 1239–1249.

703 Heather LC, Hafstad AD, Halade GV, Harmancey R, Mellor KM, Mishra PK, Mulvihill EE, Nabben M,
704 Nakamura M, Rider OJ, Ruiz M, Wende AR & Ussher JR (2022). Guidelines on models of diabetic
705 heart disease. *Am J Physiol Heart Circ Physiol* **323,** H176–H200.

706 van Heerebeek L, Borbély A, Niessen HWM, Bronzwaer JGF, van der Velden J, Stienen GJM, Linke WA,
707 Laarman GJ & Paulus WJ (2006). Myocardial Structure and Function Differ in Systolic and Diastolic
708 Heart Failure. *Circulation* **113,** 1966–1973.

709 Helmes M, Najafi A, Palmer BM, Breel E, Rijnveld N, Iannuzzi D & van der Velden J (2016). Mimicking the
710 cardiac cycle in intact cardiomyocytes using diastolic and systolic force clamps; measuring power
711 output. *Cardiovasc Res* **111,** 66–73.

712 Hopf A-E, Andresen C, Kötter S, Isić M, Ulrich K, Sahin S, Bongardt S, Röll W, Drove F, Scheerer N,
713 Vandekerckhove L, De Keulenaer GW, Hamdani N, Linke WA & Krüger M (2018). Diabetes-Induced
714 Cardiomyocyte Passive Stiffening Is Caused by Impaired Insulin-Dependent Titin Modification and
715 Can Be Modulated by Neuregulin-1. *Circulation Research* **123,** 342–355.

716 Howlett SE, Grandy SA & Ferrier GR (2006). Calcium spark properties in ventricular myocytes are altered in
717 aged mice. *American Journal of Physiology-Heart and Circulatory Physiology* **290,** H1566–H1574.

718 Jackson AM et al. (2022). Diabetes and pre-diabetes in patients with heart failure and preserved ejection
719 fraction. *Eur J Heart Fail* **24,** 497–509.

720 Janssens JV, Ma B, Brimble MA, Van Eyk JE, Delbridge LMD & Mellor KM (2018). Cardiac troponins may be
721 irreversibly modified by glycation: novel potential mechanisms of cardiac performance modulation.
722 *Sci Rep* **8,** 16084.

723 Janssens JV, Raaijmakers AJA, Weeks KL, Bell JR, Mellor KM, Curl CL & Delbridge LMD (2024). The
724 cardiomyocyte origins of diastolic dysfunction: cellular components of myocardial stiffness. *Am J*
725 *Physiol Heart Circ Physiol*; DOI: 10.1152/ajpheart.00334.2023.

726 Kamon T, Kaneko H, Itoh H, Kiriyama H, Koyama K, Fujiu K, Morita H, Uno K, Hayashi N & Komuro I (2020).
727 Association between insulin resistance and left ventricular diastolic dysfunction in non-diabetic
728 general population. *European Heart Journal* **41,** ehaa946.3057.

729 Kilfoil PJ, Lotteau S, Zhang R, Yue X, Aynaszyan S, Solymani RE, Cingolani E, Marbán E & Goldhaber JI (2020).
730 Distinct features of calcium handling and β-adrenergic sensitivity in heart failure with preserved
731 versus reduced ejection fraction. *J Physiol* **598,** 5091–5108.

732 Kittleson MM, Panjrath GS, Amancherla K, Davis LL, Deswal A, Dixon DL, Januzzi JL & Yancy CW (2023). 2023
733 ACC Expert Consensus Decision Pathway on Management of Heart Failure With Preserved Ejection
734 Fraction: A Report of the American College of Cardiology Solution Set Oversight Committee. *Journal*
735 *of the American College of Cardiology* **81,** 1835–1878.

736 Lab MJ, Allen DG & Orchard CH (1984). The effects of shortening on myoplasmic calcium concentration and
737 on the action potential in mammalian ventricular muscle. *Circulation Research* **55,** 825–829.

738 Lam CSP, Arnott C, Beale AL, Chandramouli C, Hilfiker-Kleiner D, Kaye DM, Ky B, Santema BT, Sliwa K &
739 Voors AA (2019). Sex differences in heart failure. *European Heart Journal* **40,** 3859–3868c.

740 Leopoldo AS, Sugizaki MM, Lima-Leopoldo AP, do Nascimento AF, de Azevedo Melo Luvizotto R, de Campos
741 DHS, Okoshi K, Pai-Silva MD, Padovani CR & Cicogna AC (2010). Cardiac remodeling in a rat model
742 of diet-induced obesity. *Can J Cardiol* **26,** 423–429.

743 Leung M, Phan V, Whatmough M, Heritier S, Wong VW & Leung DY (2015). Left ventricular diastolic reserve
744 in patients with type 2 diabetes mellitus. *Open Heart* **2,** e000214.

745 Lo Q & Thomas L (2010). Echocardiographic evaluation of diastolic heart failure. *Australas J Ultrasound Med*
746 **13,** 14–26.

747 Loescher CM, Freundt JK, Unger A, Hessel AL, Kühn M, Koser F & Linke WA (2023). Titin governs myocardial
748 passive stiffness with major support from microtubules and actin and the extracellular matrix. *Nat*
749 *Cardiovasc Res* **2,** 991–1002.

750 Louch WE (2020). A horse of a different colour: distinct mechanisms of HFpEF and HFrEF. *J Physiol* **598,**
751 5005–5006.

752 Luo M & Anderson ME (2013). Mechanisms of altered Ca^{2+} handling in heart failure. *Circ Res* **113,** 690–708.

753 McHugh K, DeVore AD, Wu J, Matsouaka RA, Fonarow GC, Heidenreich PA, Yancy CW, Green JB, Altman N
754 & Hernandez AF (2019). Heart Failure With Preserved Ejection Fraction and Diabetes: JACC State-
755 of-the-Art Review. *J Am Coll Cardiol* **73,** 602–611.

756 Mellor KM, Bell JR, Young MJ, Ritchie RH & Delbridge LMD (2011). Myocardial autophagy activation and
757 suppressed survival signaling is associated with insulin resistance in fructose-fed mice. *Journal of*
758 *Molecular and Cellular Cardiology* **50,** 1035–1043.

759 Mellor KM, Wendt IR, Ritchie RH & Delbridge LMD (2012). Fructose diet treatment in mice induces
760 fundamental disturbance of cardiomyocyte Ca2+ handling and myofilament responsiveness. *Am J*
761 *Physiol Heart Circ Physiol* **302,** H964-972.

762 Methawasin M, Farman GP, Granzier-Nakajima S, Strom J, Kiss B, Smith JE & Granzier H (2022). Shortening
763 the thick filament by partial deletion of titin's C-zone alters cardiac function by reducing the
764 operating sarcomere length range. *J Mol Cell Cardiol* **165,** 103–114.

765 Mirsky I (1976). Assessment of passive elastic stiffness of cardiac muscle: mathematical concepts,
766 physiologic and clinical considerations, directions of future research. *Prog Cardiovasc Dis* **18,** 277–
767 308.

768 Najafi A, van de Locht M, Schuldt M, Schönleitner P, van Willigenburg M, Bollen I, Goebel M, Ottenheijm
769 CAC, van der Velden J, Helmes M & Kuster DWD (2019). End-diastolic force pre-activates
770 cardiomyocytes and determines contractile force: role of titin and calcium. *J Physiol* **597,** 4521–
771 4531.

772 Natali AJ, Turner DL, Harrison SM & White E (2001). Regional effects of voluntary exercise on cell size and
773 contraction-frequency responses in rat cardiac myocytes. *Journal of Experimental Biology* **204,**
774 1191–1199.

775 Patil VC, Patil HV, Shah KB, Vasani JD & Shetty P (2011). Diastolic dysfunction in asymptomatic type 2
776 diabetes mellitus with normal systolic function. *J Cardiovasc Dis Res* **2,** 213–222.

777 Peyronnet R, Bollensdorff C, Capel RA, Rog-Zielinska EA, Woods CE, Charo DN, Lookin O, Fajardo G, Ho M,
778 Quertermous T, Ashley EA & Kohl P (2017). Load-dependent effects of apelin on murine
779 cardiomyocytes. *Prog Biophys Mol Biol* **130,** 333–343.

780 Pulinilkunnil T, Kienesberger PC, Nagendran J, Sharma N, Young ME & Dyck JRB (2014). Cardiac-specific
781 adipose triglyceride lipase overexpression protects from cardiac steatosis and dilated
782 cardiomyopathy following diet-induced obesity. *Int J Obes* **38,** 205–215.

783 Redfield MM (2016). Heart Failure with Preserved Ejection Fraction. *N Engl J Med* **375,** 1868–1877.

784 Reichelt ME, Mellor KM, Bell JR, Chandramouli C, Headrick JP & Delbridge LMD (2013). Sex, sex steroids,
785 and diabetic cardiomyopathy: making the case for experimental focus. *Am J Physiol Heart Circ*
786 *Physiol* **305,** H779-792.

787 Robinson P, Liu X, Sparrow A, Patel S, Zhang Y-H, Casadei B, Watkins H & Redwood C (2018). Hypertrophic
788 cardiomyopathy mutations increase myofilament Ca2+ buffering, alter intracellular Ca2+ handling,
789 and stimulate Ca2+-dependent signaling. *J Biol Chem* **293,** 10487–10499.

790 Rozenbaum Z, Topilsky Y, Khoury S, Pereg D & Laufer-Perl M (2019). Association of body mass index and
791 diastolic function in metabolically healthy obese with preserved ejection fraction. *Int J Cardiol* **277,**
792 147–152.

793 Satoh H, Delbridge LM, Blatter LA & Bers DM (1996). Surface:volume relationship in cardiac myocytes
794 studied with confocal microscopy and membrane capacitance measurements: species-dependence
795 and developmental effects. *Biophys J* **70,** 1494–1504.

796 Shimkunas R et al. (2021). Mechanical Load Regulates Excitation-Ca2+ Signaling-Contraction in
797 Cardiomyocyte. *Circ Res* **128,** 772–774.

798 Sotomi Y et al. (2021). Sex Differences in Heart Failure With Preserved Ejection Fraction. *J Am Heart Assoc*
799 **10,** e018574.

800 Sowers JR, Habibi J, Jia G, Bostick B, Manrique-Acevedo C, Lastra G, Yang Y, Chen D, Sun Z, Domeier TL,
801 Durante W, Whaley-Connell AT, Hill MA, Jaisser F, DeMarco VG & Aroor AR (2020). Endothelial

802 sodium channel activation promotes cardiac stiffness and diastolic dysfunction in Western diet fed
803 female mice. *Metabolism* **109,** 154223.

804 Varian KD & Janssen PML (2007). Frequency-dependent acceleration of relaxation involves decreased
805 myofilament calcium sensitivity. *American Journal of Physiology-Heart and Circulatory Physiology*
806 **292,** H2212–H2219.

807 Villalobos Lizardi JC, Baranger J, Nguyen MB, Asnacios A, Malik A, Lumens J, Mertens L, Friedberg MK,
808 Simmons CA, Pernot M & Villemain O (2022). A guide for assessment of myocardial stiffness in
809 health and disease. *Nat Cardiovasc Res* **1,** 8–22.

810 Wells SP, Raaijmakers AJA, Curl CL, O'Shea C, Hayes S, Mellor KM, Kalman JM, Kirchhof P, Pavlovic D,
811 Delbridge LMD & Bell JR (2023). Localized cardiomyocyte lipid accumulation is associated with
812 slowed epicardial conduction in rats. *J Gen Physiol* **155,** e202213296.

813 White E, Boyett MR & Orchard CH (1995). The effects of mechanical loading and changes of length on single
814 guinea-pig ventricular myocytes. *The Journal of Physiology* **482,** 93–107.

815 Wingard MC, Dalal S, Shook PL, Myers R, Connelly BA, Thewke DP, Singh M & Singh K (2021). Deficiency of
816 ataxia-telangiectasia mutated kinase modulates functional and biochemical parameters of the
817 heart in response to Western-type diet. *Am J Physiol Heart Circ Physiol* **320,** H2324–H2338.

818 Zhou P & Pu WT (2016). Recounting Cardiac Cellular Composition. *Circulation Research* **118,** 368–370.

819

820 **FIGURE LEGENDS**

821 **Fig.1 Systemic indicators of cardiometabolic disease and *in vivo* diastolic function in high-fat/sugar diet**
822 **(HFSD) vs control (CTRL) mice**.
823 **A**. Body weight elevation at 5 week intervals up to 25 weeks of dietary treatment (last timepoint full cohort
824 intact. N = 16 – 17 mice per group).
825 **B.** Glucose tolerance testing at 23-24 weeks post dietary intervention; N = 6 mice per group).
826 **C**. Echocardiography exemplar blood flow and tissue doppler images from which diastolic indices were
827 derived for CTRL and HFSD mice. Upper panels: HFSD mitral blood flow & annular wall motion. Lower
828 panels: CTRL mitral blood flow & annular wall motion. (N = 9-16 mice per group)
829 **D**. Early diastolic mitral annular blood flow (E) was increased in HFSD.
830 **E.** Early diastolic mitral annular wall velocity (e') was decreased in HFSD.
831 **F.** Deceleration time of early diastolic mitral annular blood flow was decreased in HFSD.
832 **G.** Ratio of early diastolic blood flow to wall velocity (E/e') was increased in HFSD.
833
834 Time-course data analysed using two-way repeated measures ANOVA with Sidak post-hoc test (*p < 0.05).
835 Comparisons between two treatment groups performed using student's t-test; *p<0.05, **p<0.01,
836 ***p<0.001). Data presented as mean ± standard error of the mean.
837
838
839 **Fig.2 Comparing non-loaded sarcomere shortening and lengthening in CTRL and HFSD cardiomyocytes**.
840 **A.** Mean sarcomere contraction cycles presented as a percentage of diastolic sarcomere length for CTRL
841 and HFSD cardiomyocytes
842 **B-C.** Mean diastolic sarcomere length and peak sarcomere shortening for CTRL and HFSD cardiomyocytes.
843 **D.** Mean sarcomere shortening and lengthening rate records (time derivative of sarcomere contraction-
844 relaxation cycle) for CTRL and HFSD cardiomyocytes. The nadir and zenith represent maximal shortening
845 and lengthening rates respectively.
846 **E-F.** Maximal rate of lengthening and shortening rates for CTRL and HFSD cardiomyocytes.
847
848 Mean data computed from average of 20 cycles per cardiomyocyte to derive group mean (N = 7-8 mice per
849 group, n = 38-47 cells per group). Comparisons between two treatment groups performed using student's
850 t-test (all p>0.05, ns). Data presented as mean ± standard error of the mean.
851
852
853 **Fig. 3 Ca^{2+} signals in non-loaded (isotonic) paced cardiomyocytes.**
854 **A-B.** Mean diastolic Ca^{2+} levels and time constant of transient decay (*tau*) in HFSD and CTRL
855 cardiomyocytes.
856 **C-D.** Mean systolic Ca^{2+} levels and amplitude of the Ca^{2+} transient for CTRL and HFSD.
857 **E.** Mean Ca^{2+} transient records for CTRL and HFSD cardiomyocytes.
858
859 Mean data computed from average of 20 cycles per cardiomyocyte to derive group mean (N = 6-8 mice per
860 group, n = 32-37 cells per group). Comparisons between treatment groups were performed using Student's
861 t-test; *p<0.05). Data presented as mean ± standard error of the mean.
862

Fig. 4 Sarcomere shortening and lengthening in non-loaded (isotonic) and loaded (auxotonic) pacing states.

A. Exemplar non-loaded (isotonic) and loaded (auxotonic) sarcomere contraction cycles for the same cardiomyocyte (CTRL).

B-C. Peak sarcomere shortening and maximum rate of lengthening, measured for each cardiomyocyte in non-loaded (isotonic) and loaded (auxotonic) state for CTRL and HFSD groups combined (N = 9 mice, n = 25 cells). Mean data for CTRL and HFSD are presented as grey points to the left (non-loaded) and right (loaded) of individual cardiomyocyte data.

D. Correlation of loading associated peak sarcomere shortening change and maximum rate of lengthening change for CTRL and HFSD combined.

E. Mean sarcomere loading effect on maximum lengthening rate (µm/s) normalized by shortening extent (µm) for CTRL vs HFSD. (CTRL: N = 5 mice, n = 13 cells; HFSD: N = 4 mice, n = 12 cells). Significant ANOVA interaction effect (diet treatment x load state).

F. Mean decrement in maximum sarcomere lengthening rate (µm/s) normalized by shortening extent (µm).

Comparison of cardiomyocyte responses in different loading conditions analysed by paired t-test. Comparison of cardiomyocytes from different treatment groups analysed by unpaired t-test. A 2-way ANOVA with repeated measures used for analysis of two independent variables Data fitted with linear regression model and calculation of Pearson's correlation coefficient. Data presented as mean ± standard error of the mean. *p<0.05, **p<0.01, ****p<0.0001, #p<0.05 ANOVA factor interaction.

Fig. 5 Quantifying diastolic stiffness in CTRL vs HFSD cardiomyocytes using strain normalization methods

A. Exemplar stress recordings of CTRL and HFSD cardiomyocytes undergoing 'stress-length' protocol (2Hz paced). Diastolic baseline stress shifts indicated by broken line.

B. Diastolic and systolic sarcomere mean stress-length relations in CTRL cardiomyocytes (N = 5 mice, n = 9 cells).

C. Diastolic sarcomere mean stress-length relation (linear regression fit) for HFSD and CTRL.

D. Diastolic stress (mN/mm^2) normalized relative to sarcomere stretch (µm) yields sarcomere stress/strain = stiffness [(mN/mm^2) /strain (µm)] for HFSD and CTRL.

E. Diastolic mean cardiomyocyte segment stress-length relation (linear regression fit) for HFSD and CTRL..

F. Diastolic stress (mN/mm^2) normalized relative to segment stretch (% length) yields cardiomyocyte segment stress/strain = stiffness [(mN/mm^2) /strain (% length)] for HFSD & CTRL.

G. Correlation (linear regression fit) of *in vitro* cardiomyocyte segment diastolic stiffness (stress/strain) with *in vivo* diastolic dysfunction E/e' (blood flow/wall motion) in CTRL and HFSD. Cardiomyocyte data averaged per heart.

Comparisons between two groups performed using student's t-test (*p<0.05, **p<0.01). Data fitted with linear regression model and calculation of Pearson's correlation coefficient, presented as mean ± standard error of the mean. For **C. & D.** (CTRL: N=5 mice, n=9 cells; HFSD: N=2 mice, n=7 cells). For **E.&F.** (CTRL: N=6 mice, n = 16 cells; HFSD: N=6 mice, n=18 cells).

905 **Fig. 6 Load dependence of cardiomyocyte Ca^{2+} transient decay in CTRL and HFSD cardiomyocytes.**
906 **A-B.** Exemplar Ca^{2+} transient decay records, with a mono-exponential decay function fit, in non-loaded
907 (isotonic) and loaded (auxotonic, stretched) CTRL and HFSD cardiomyocytes. Horizontal black broken lines
908 intersect with mono-exponential fit at 36.8% (1/e) transient amplitude. Vertical broken lines from
909 intersection points indicate the time constant of Ca^{2+} transient decay (tau).
910 **C.** Time constant of Ca^{2+} transient decay (tau) in cardiomyocytes with different load conditions: auxotonic
911 (aux) & stretched (str) shown as fold change relative to non-loaded isotonic (iso) for CTRL and HFSD.
912
913 For analysis of two independent variables a 2-way ANOVA with repeated measures used (CTRL: N = 5 mice,
914 n = 13 cells; HFSD: N = 4 mice, n = 12 cells). Data are presented as mean ± standard error of the mean.
915 ***p<0.001 (HFSD stretched vs non-loaded isotonic). Non-significant ANOVA interaction effect (p = 0.055,
916 diet treatment x load state).
917
918
919 **Fig. 7 Pacing induced changes in cardiomyocyte cytosolic Ca^{2+} levels and stiffness in CTRL & HFSD.**
920 **A.** Exemplar CTRL and HFSD cardiomyocyte Ca^{2+} transients at 2 and 4 Hz pacing.
921 **B.** Diastolic cardiomyocyte Ca^{2+} levels measured before and after transition from 2 to 4 Hz pacing in HFSD &
922 CTRL.
923 **C.** Diastolic cardiomyocyte Ca^{2+} level mean shift with transition from 2 to 4 Hz pacing in HFSD & CTRL.
924 **D.** Diastolic sarcomere length measured before and after transition from 2 to 4 Hz pacing in HFSD & CTRL.
925 **E.** Diastolic mean cardiomyocyte segment stress-length relation (linear regression fit) for HFSD and CTRL at
926 2 and 4 Hz pacing.
927 **F.** Diastolic mean cardiomyocyte segment stress-length relation slope (mN/mm^2) normalized relative to
928 segment stretch (% length) yields cardiomyocyte mean segment stress/strain = stiffness [(mN/mm^2) /strain
929 (% length)] for HFSD and CTRL at 2 and 4 Hz pacing.
930
931 Comparison between two groups performed using unpaired t-test. With two independent variables a
932 repeated measures 2-way ANOVA Sidaks post-hoc analysis was performed (*p<0.05, **p<0.01,
933 ****p<0.0001). Data are presented as mean ± standard error of the mean or mean with paired individual
934 points. For **B. & C.** (CTRL: N = 4 mice, n = 9 cells; HFSD: N = 4 mice, n = 8 cells). For **D. & E.** (CTRL: N = 4 mice,
935 n = 7 cells; HFSD: N = 4 mice, n = 9 cells). For **F.** (CTRL: N = 4 mice, n = 8 cells; HFSD: N = 4 mice, n = 9 cells).
936

Table S1. Echocardiographic parameters in CTRL and HFSD mice.

LVIDd left ventricular internal diameter at end diastole, *IVSd* interventricular septum diameter at end diastole, *LVPWd* left ventricular posterior wall thickness at end diastole, *RWT* relative wall thickness, *E wave* mitral valve blood flow velocity during the early ventricular filling phase, *A wave* mitral valve blood flow velocity during atrial contraction, *e' wave* mitral annulus tissue motion velocity during the early ventricular filling phase, *a' wave* mitral annulus tissue motion velocity during atrial contraction, *MV Dec T* mitral valve deceleration time.

Comparisons between two treatment groups performed using Students' unpaired t-test (N = 9-15 mice per group; *$p < 0.05$, **$p<0.01$, ***$p<0.001$). Data are presented as mean ± standard error of the mean.

Fig. S1. Cardiomyocyte standardized stretch protocol.

A. Image of a left ventricular cardiomyocyte longitudinally attached to glass rods. Edge-tracking used to measure inter-rod distance (marked as blue bars) for cardiomyocyte segment analyses. The delineated region of interest (marked pink) represents the area from which Fast Fourier Transform analysis of sarcomere striations was performed to derive sarcomere-specific data.

B. Exemplar traces depict the change in glass rod internal distance in response to successive 0.5V piezo motor inputs used for calibration of stretch protocol for each individual cardiomyocyte to allow normalized comparisons.

C. Measuring stress and strain during progressive cardiomyocyte stretch. Exemplar force, sarcomere length and rod edge-tracker traces during the first stretch of a stress-length protocol.

D. Comparison of variability of cell stretches performed using a uniform (preset) stretch constant and the individually derived stretch calibration constant. Reproducibility is optimized using the individual stretch calibration constant. Data shown as median ± interquartile range.

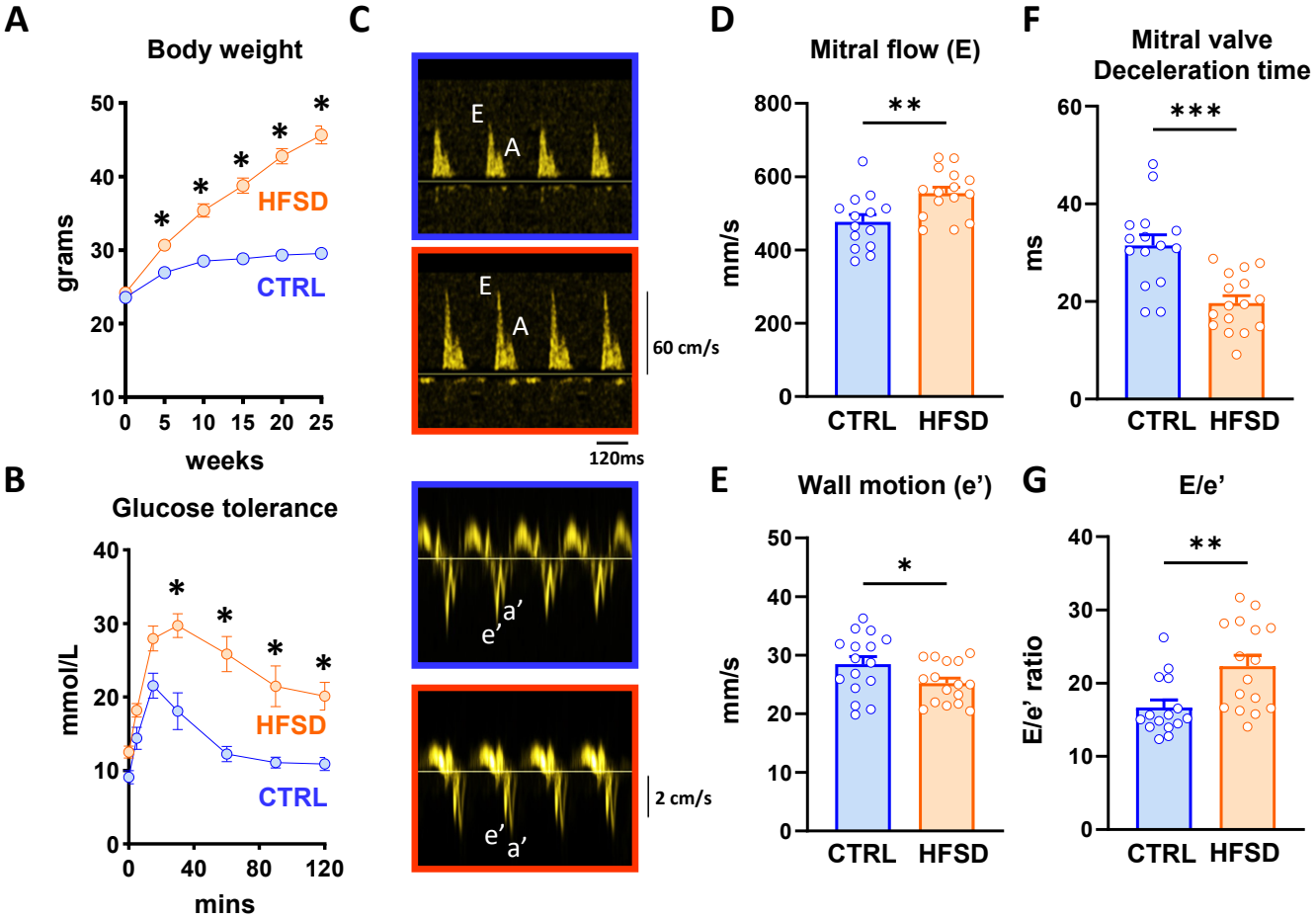

Fig.1 Systemic indicators of cardiometabolic disease and *in vivo* diastolic function in high-fat/sugar diet (HFSD) vs control (CTRL) mice.

A. Body weight elevation at 5 week intervals up to 25 weeks of dietary treatment (last timepoint full cohort intact. N = 16 – 17 mice per group).

B. Glucose tolerance testing at 23-24 weeks post dietary intervention; N = 6 mice per group).

C. Echocardiography exemplar blood flow and tissue doppler images from which diastolic indices were derived for CTRL and HFSD mice. Upper panels: HFSD mitral blood flow & annular wall motion. Lower panels: CTRL mitral blood flow & annular wall motion. (N = 14-16 mice per group)

D. Early diastolic mitral annular blood flow (E) was increased in HFSD.

E. Early diastolic mitral annular wall velocity (e') was decreased in HFSD.

F. Deceleration time of early diastolic mitral annular blood flow was decreased in HFSD.

G. Ratio of early diastolic blood flow to wall velocity (E/e') was increased in HFSD.

Time-course data analysed using two-way repeated measures ANOVA with Sidak post-hoc test (*$p < 0.05$). Comparisons between two treatment groups performed using student's t-test; *$p<0.05$, **$p<0.01$, ***$p<0.001$). Data presented as mean ± standard error of the mean.

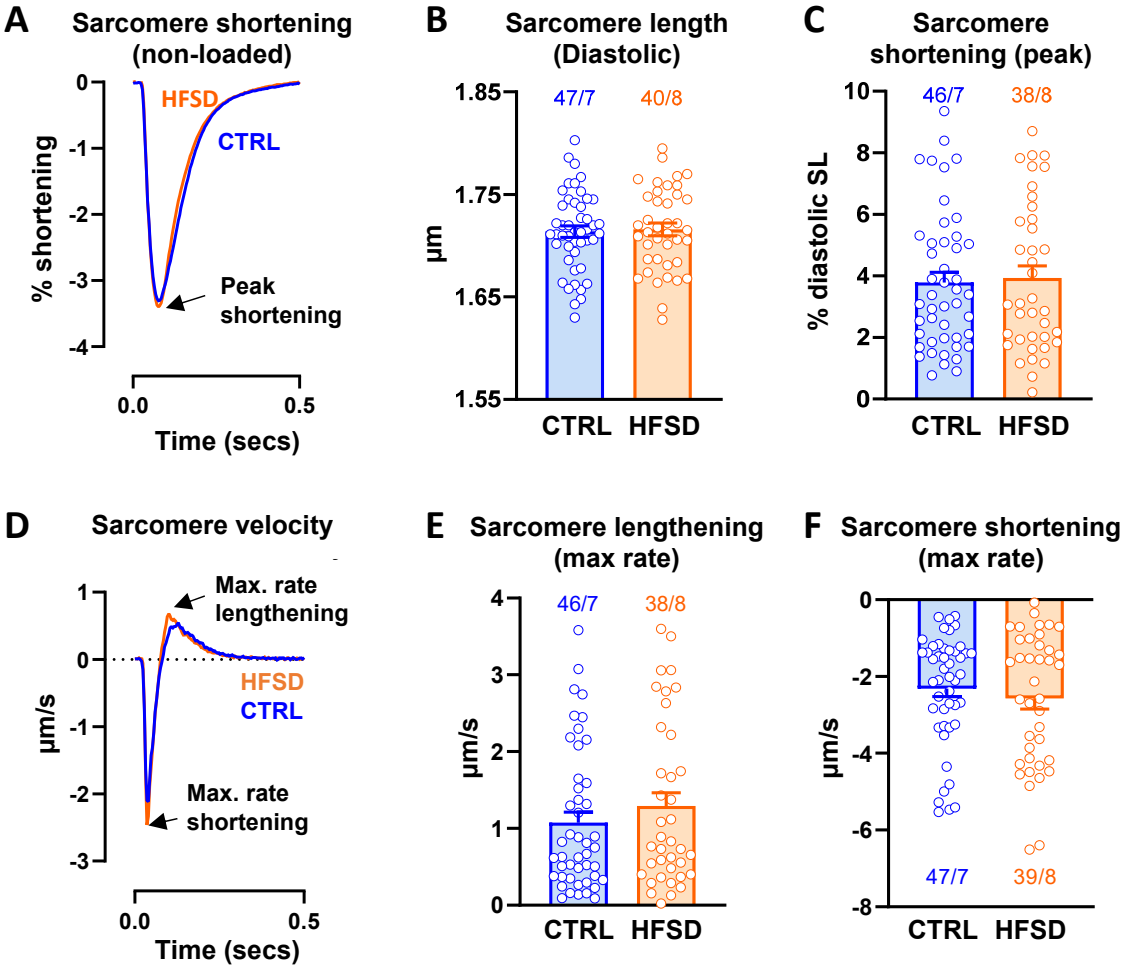

Fig.2 Comparing non-loaded sarcomere shortening and lengthening in CTRL and HFSD cardiomyocytes.
A. Mean sarcomere contraction cycles presented as a percentage of diastolic sarcomere length for CTRL and HFSD cardiomyocytes
B-C. Mean diastolic sarcomere length and peak sarcomere shortening for CTRL and HFSD cardiomyocytes.
D. Mean sarcomere shortening and lengthening rate records (time derivative of sarcomere contraction-relaxation cycle) for CTRL and HFSD cardiomyocytes. The nadir and zenith represent maximal shortening and lengthening rates respectively.
E-F. Maximal rate of lengthening and shortening rates for CTRL and HFSD cardiomyocytes.

Mean data computed from average of 20 cycles per cardiomyocyte to derive group mean (N = 7-8 mice per group, n = 38-47 cells per group). Comparisons between two treatment groups performed using student's t-test (all p>0.05, ns). Data presented as mean ± standard error of the mean.

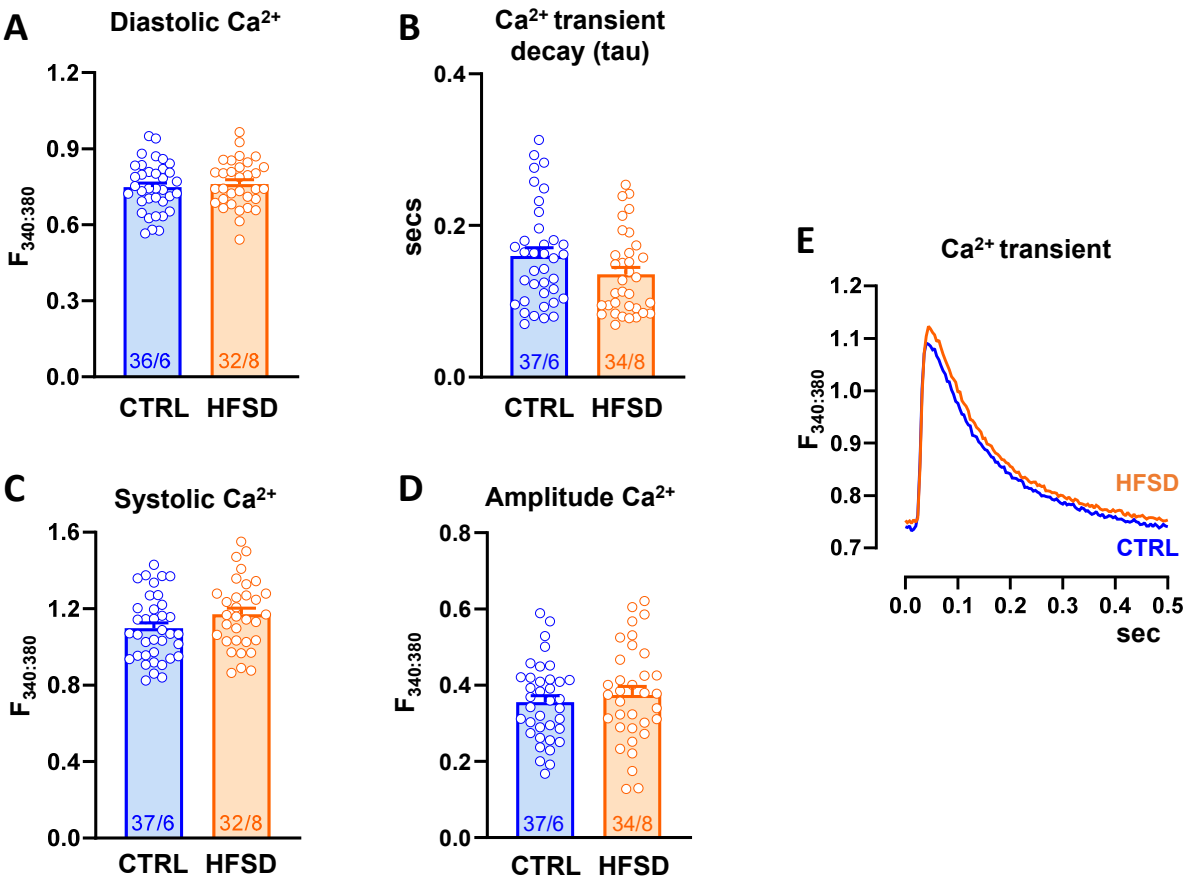

Fig. 3 Ca^{2+} signals in non-loaded (isotonic) paced cardiomyocytes.
A-B. Mean diastolic Ca^{2+} levels and time constant of transient decay (*tau*) in HFSD and CTRL cardiomyocytes.
C-D. Mean systolic Ca^{2+} levels and amplitude of the Ca^{2+} transient for CTRL and HFSD.
E. Mean Ca^{2+} transient records for CTRL and HFSD cardiomyocytes.

Mean data computed from average of 20 cycles per cardiomyocyte to derive group mean (N = 6-8 mice per group, n = 32-37 cells per group). Comparisons between treatment groups were performed using Student's t-test; *$p<0.05$). Data presented as mean ± standard error of the mean.

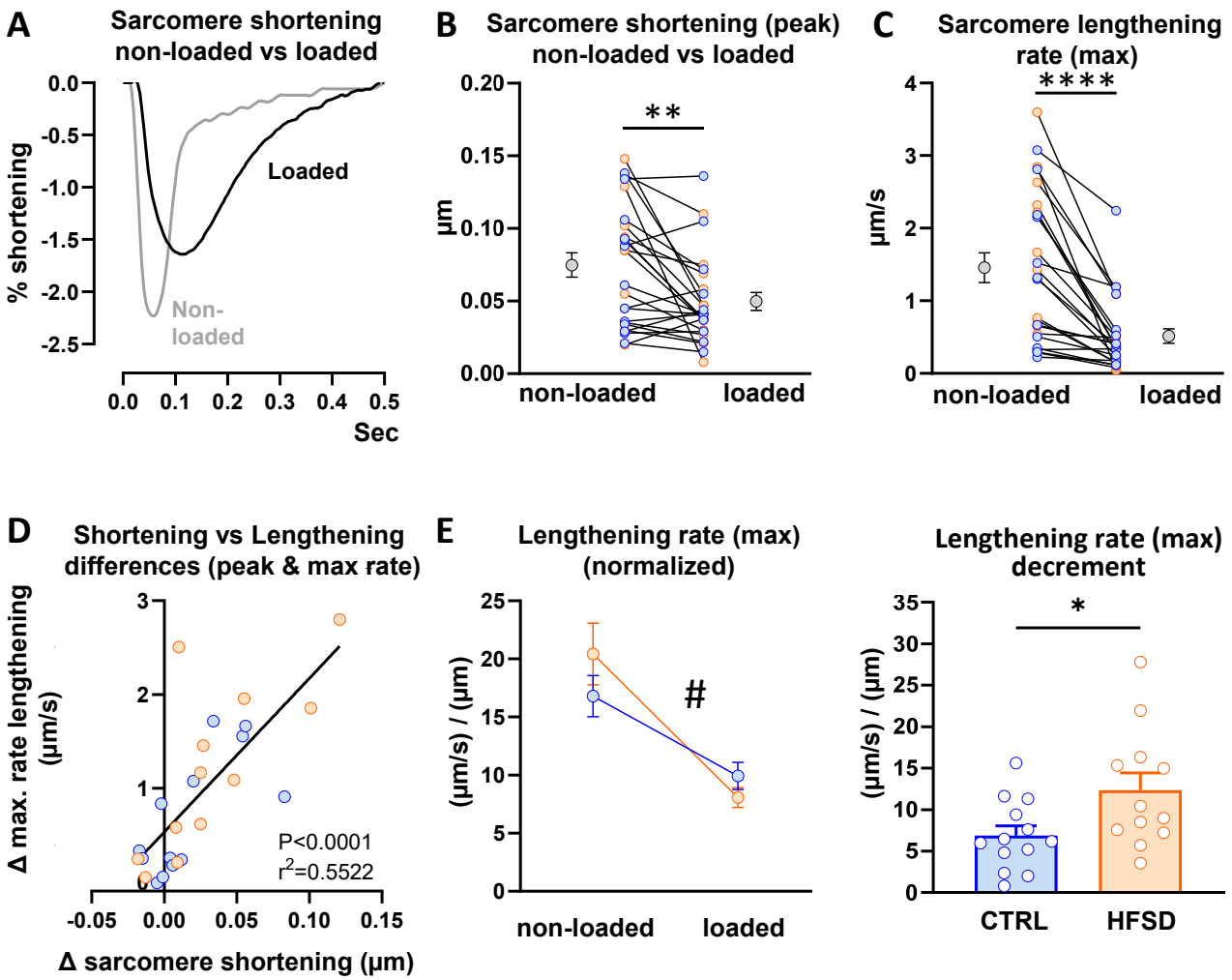

Fig. 4 Sarcomere shortening and lengthening in non-loaded (isotonic) and loaded (auxotonic) pacing states.

A. Exemplar non-loaded (isotonic) and loaded (auxotonic) sarcomere contraction cycles for the same cardiomyocyte (CTRL).

B-C. Peak sarcomere shortening and maximum rate of lengthening, measured for each cardiomyocyte in non-loaded (isotonic) and loaded (auxotonic) state for CTRL and HFSD groups combined (N = 9 mice, n = 25 cells). Mean data for CTRL and HFSD are presented as grey points to the left (non-loaded) and right (loaded) of individual cardiomyocyte data.

D. Correlation of loading associated peak sarcomere shortening change and maximum rate of lengthening change for CTRL and HFSD combined.

E. Mean sarcomere loading effect on maximum lengthening rate (µm/s) normalized by shortening extent (µm) for CTRL vs HFSD. (CTRL: N = 5 mice, n = 13 cells; HFSD: N = 4 mice, n = 12 cells). Significant ANOVA interaction effect (diet treatment x load state).

F. Mean decrement in maximum sarcomere lengthening rate (µm/s) normalized by shortening extent (µm).

Comparison of cardiomyocyte responses in different loading conditions analysed by paired t-test. Comparison of cardiomyocytes from different treatment groups analysed by unpaired t-test. A 2-way ANOVA with repeated measures used for analysis of two independent variables. Data fitted with linear regression model and calculation of Pearson's correlation coefficient. Data presented as mean ± standard error of the mean. *p<0.05, **p<0.01, ****p<0.0001, #p<0.05 ANOVA factor interaction.

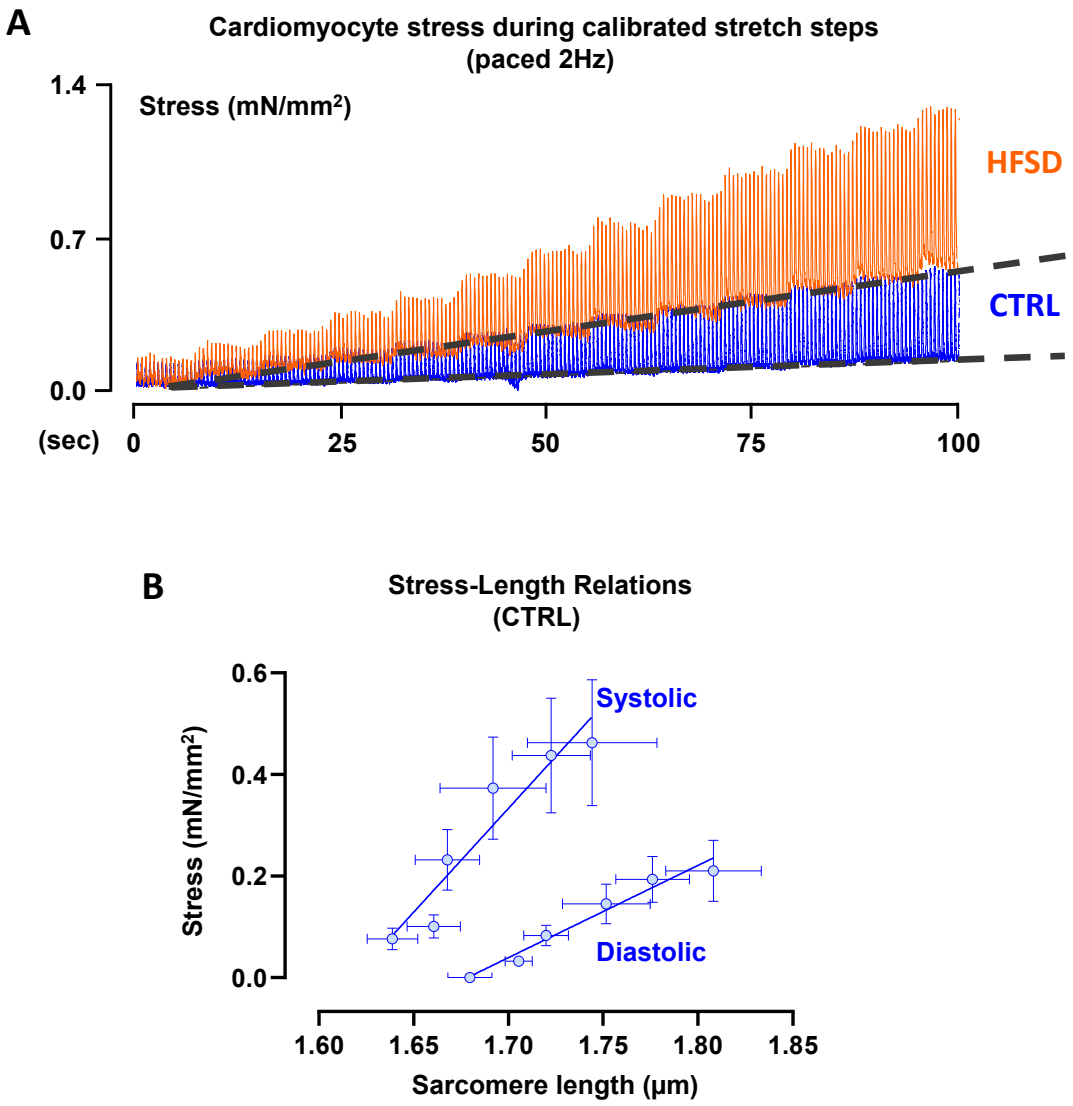

Fig. 5 Cardiomyocyte stress recordings and stress-length relations using strain normalization methods
A. Exemplar stress recordings of CTRL and HFSD cardiomyocytes undergoing 'stress-length' protocol (2Hz paced). Diastolic baseline stress shifts indicated by broken line.
B. Diastolic and systolic sarcomere mean stress-length relations in CTRL cardiomyocytes (N = 5 mice, n = 9 cells).

Data fitted with linear regression model. Data presented as mean ± standard error of the mean.

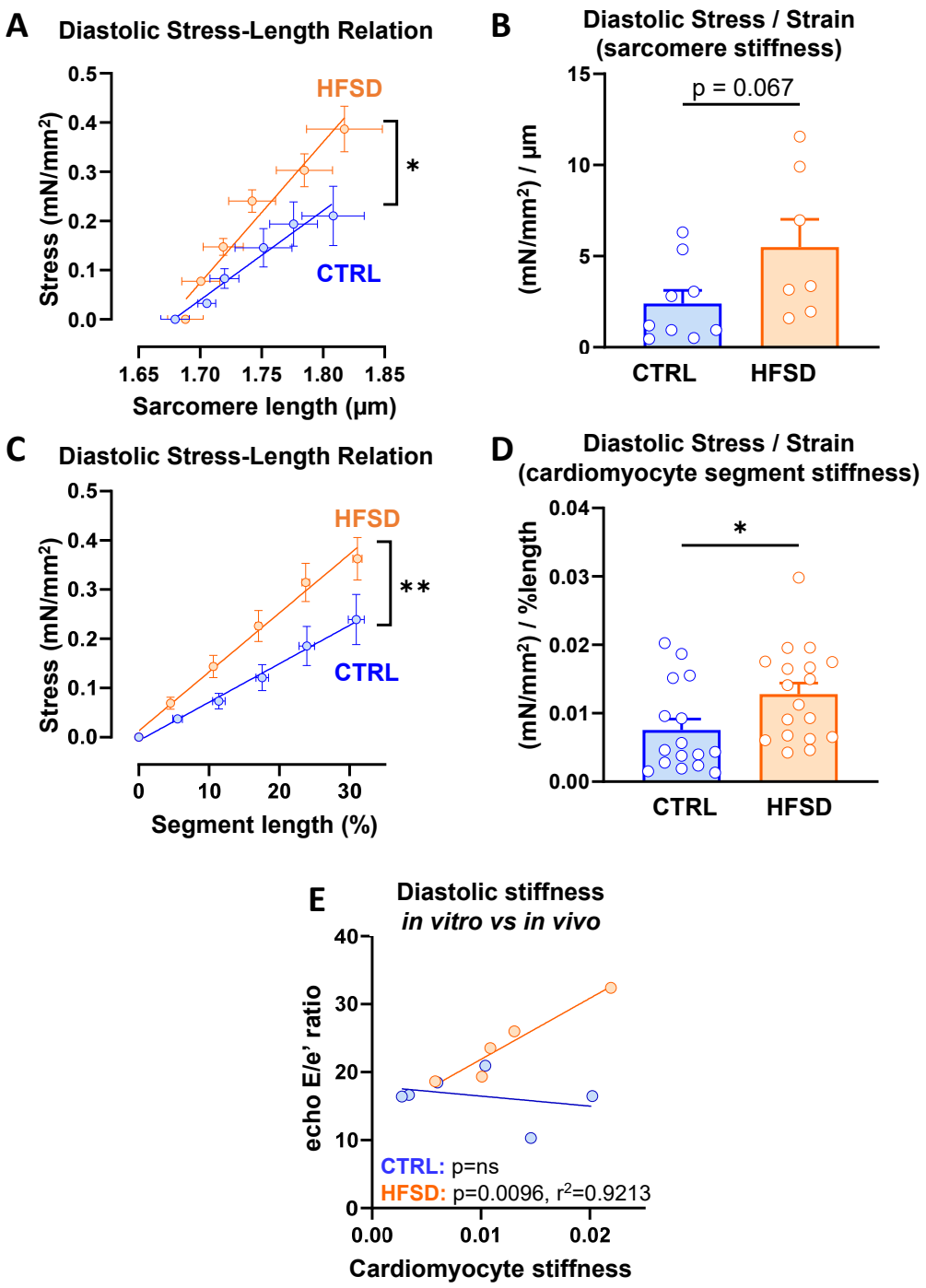

Fig. 6 Quantifying diastolic stiffness in CTRL vs HFSD cardiomyocytes using strain normalization methods (cont).

A. Diastolic sarcomere mean stress-length relation (linear regression fit) for HFSD and CTRL.

B. Diastolic stress (mN/mm^2) normalized relative to sarcomere stretch (µm) yields sarcomere stress/strain = stiffness [(mN/mm^2) /strain (µm)] for HFSD and CTRL.

C. Diastolic mean cardiomyocyte segment stress-length relation (linear regression fit) for HFSD and CTRL..

D. Diastolic stress (mN/mm^2) normalized relative to segment stretch (% length) yields cardiomyocyte segment stress/strain = stiffness [(mN/mm^2) /strain (% length)] for HFSD & CTRL.

E. Correlation (linear regression fit) of *in vitro* cardiomyocyte segment diastolic stiffness (stress/strain) with *in vivo* diastolic dysfunction E/e' (blood flow/wall motion) in CTRL and HFSD. Cardiomyocyte data averaged per heart.

Comparisons between two groups performed using student's t-test (*p<0.05, **p<0.01). Data fitted with linear regression model and calculation of Pearson's correlation coefficient, presented as mean ± standard error of the mean. For **A. & B.** (CTRL: N=5 mice, n=9 cells; HFSD: N=2 mice, n=7 cells). For **C.&D.** (CTRL: N=6 mice, n = 16 cells; HFSD: N=6 mice, n=18 cells).

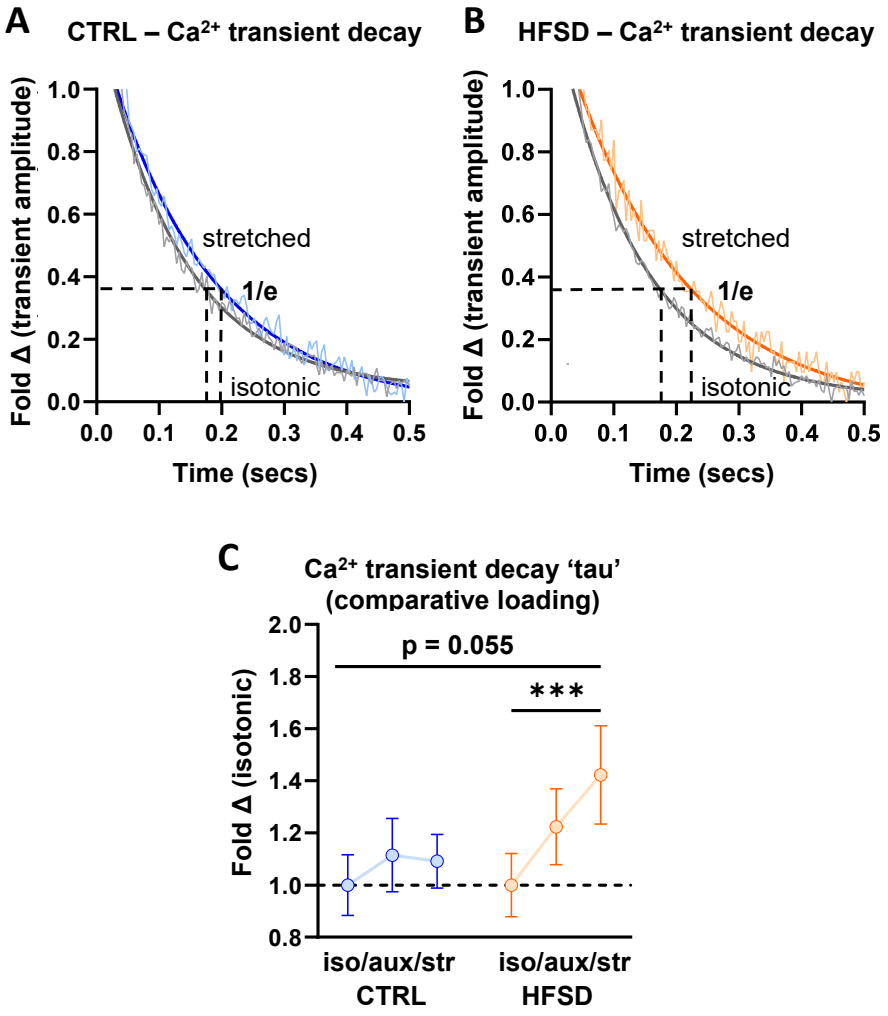

Fig. 7 Load dependence of cardiomyocyte Ca^{2+} transient decay in CTRL and HFSD cardiomyocytes.

A-B. Exemplar Ca^{2+} transient decay records, with a mono-exponential decay function fit, in non-loaded (isotonic) and loaded (auxotonic, stretched) CTRL and HFSD cardiomyocytes. Horizontal black broken lines intersect with mono-exponential fit at 36.8% (1/e) transient amplitude. Vertical broken lines from intersection points indicate the time constant of Ca^{2+} transient decay (tau).
C. Time constant of Ca^{2+} transient decay (tau) in cardiomyocytes with different load conditions: auxotonic (aux) & stretched (str) shown as fold change relative to non-loaded isotonic (iso) for CTRL and HFSD.

For analysis of two independent variables a 2-way ANOVA with repeated measures used (CTRL: N = 5 mice, n = 13 cells; HFSD: N = 4 mice, n = 12 cells). Data are presented as mean ± standard error of the mean. ***$p<0.001$ (HFSD stretched vs non-loaded isotonic). Non-significant ANOVA interaction effect ($p = 0.055$, diet treatment x load state).

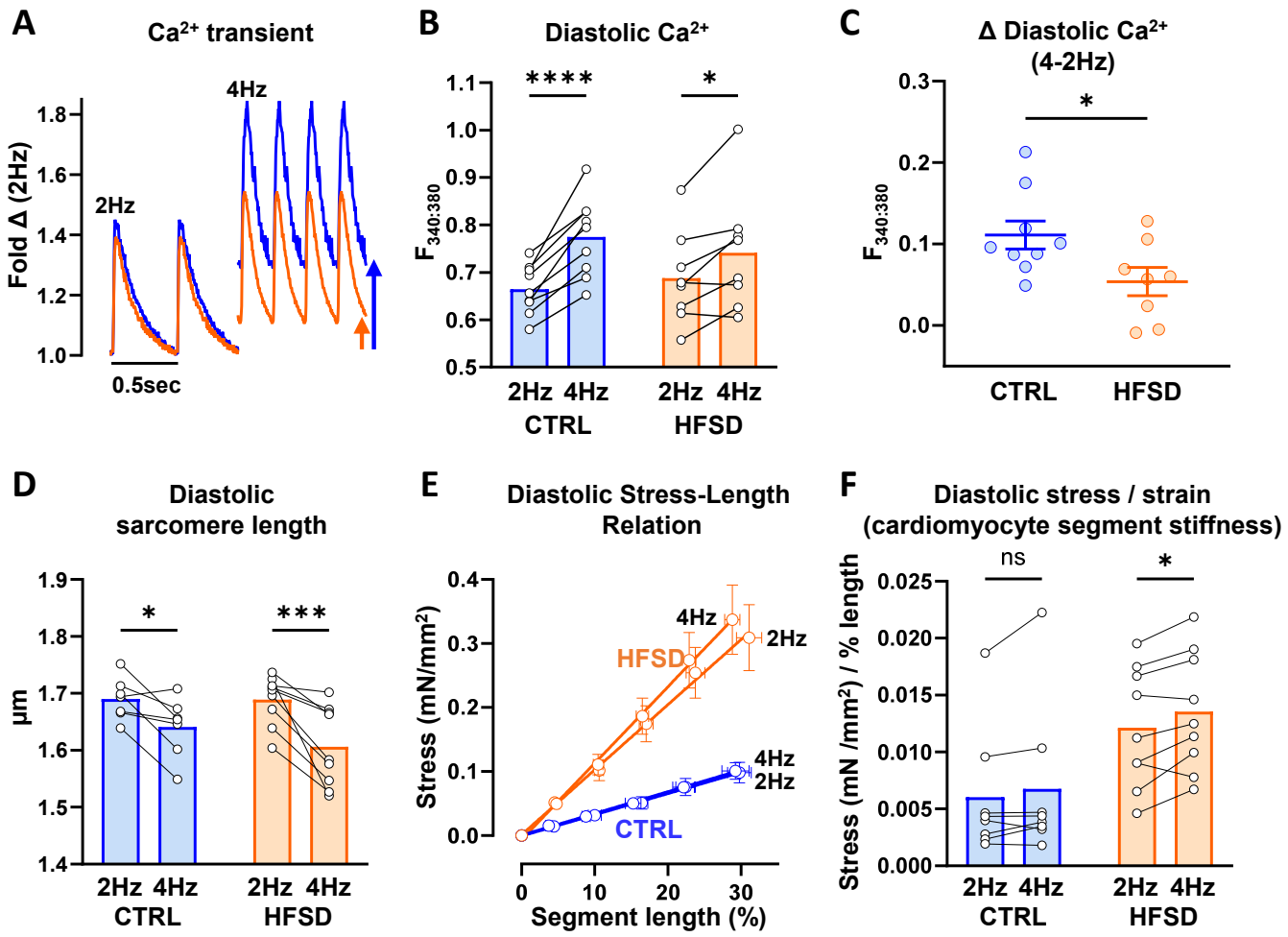

Fig. 8 Pacing induced changes in cardiomyocyte cytosolic Ca^{2+} levels and stiffness in CTRL & HFSD.
A. Exemplar CTRL and HFSD cardiomyocyte Ca^{2+} transients at 2 and 4 Hz pacing.
B. Diastolic cardiomyocyte Ca^{2+} levels measured before and after transition from 2 to 4 Hz pacing in HFSD & CTRL.
C. Diastolic cardiomyocyte Ca^{2+} level mean shift with transition from 2 to 4 Hz pacing in HFSD & CTRL.
D. Diastolic sarcomere length measured before and after transition from 2 to 4 Hz pacing in HFSD & CTRL.
E. Diastolic mean cardiomyocyte segment stress-length relation (linear regression fit) for HFSD and CTRL at 2 and 4 Hz pacing.
F. Diastolic mean cardiomyocyte segment stress-length relation slope (mN/mm^2) normalized relative to segment stretch (% length) yields cardiomyocyte mean segment stress/strain = stiffness [(mN/mm^2) /strain (% length)] for HFSD and CTRL at 2 and 4 Hz pacing.

Comparison between two groups performed using unpaired t-test. With two independent variables a repeated measures 2-way ANOVA Sidaks post-hoc analysis was performed (*$p<0.05$, **$p<0.01$, ****$p<0.0001$). Data are presented as mean ± standard error of the mean or mean with paired individual points. For **B. & C.** (CTRL: N = 4 mice, n = 9 cells; HFSD: N = 4 mice, n = 8 cells). For **D. & E.** (CTRL: N = 4 mice, n = 7 cells; HFSD: N = 4 mice, n = 9 cells). For **F.** (CTRL: N = 4 mice, n = 8 cells; HFSD: N = 4 mice, n = 9 cells).